2023-01-0919 Published 11 Apr 2023

The Influence of Traffic Wakes on the Aerodynamic Performance of Heavy Duty Vehicles

Brian McAuliffe, Hali Barber, and Faegheh Ghorbanishohrat National Research Council Canada

Citation: McAuliffe, B., Barber, H., and Ghorbanishohrat, F., "The Influence of Traffic Wakes on the Aerodynamic Performance of Heavy Duty Vehicles," *SAE Int. J. Advances & Curr. Prac. in Mobility* 5(6):2193-2214, 2023, doi:10.4271/2023-01-0919.

This article was presented at the WCX SAE World Congress Experience, April 18-20, 2023.

Received: 08 Nov 2022 Revised: 12 Jan 2023 Accepted: 01 Feb 2023

Abstract

Road vehicles have been shown to experience measurable changes in aerodynamic performance when travelling in everyday safe-distance driving conditions, with a major contributor being the lower effective wind speed associated with the wakes from forward vehicles. Using a novel traffic-wake-generator system, a comprehensive test program was undertaken to examine the influence of traffic wakes on the aerodynamic performance of heavy-duty vehicles (HDVs). The experiments were conducted in a large wind tunnel with four primary variants of a high-fidelity 30%-scale tractor-trailer model. Three high-roof-tractor models (conventional North-American sleeper-cab and day-cab, and a zero-emissions-cab style) paired with a standard dry-van trailer were tested, along with a low-roof day-cab tractor paired with a flat-bed trailer. Amongst these, trailer variants provided a total of 10 HDV configurations that were tested in uniform turbulent flow over a range of freestream yaw angles between ±15°, and with wake effects over a range of yaw angles between -2° and +11°. Up to 53 specific wake-flow conditions were applied to each HDV configuration. Wind-load and surface-pressure measurements were acquired and provide indicators of the manner in which the aerodynamic performance of the HDV models are influenced by traffic wakes.

Drag-coefficient reductions up to 17% for individual drag-coefficient values and up to 9% for wind-averaged values were observed. Wakes from adjacent-lane vehicles were observed to have comparable, or sometimes greater, influence to those from safe-distance same-lane vehicles. The wakes influence primarily the forward-facing surfaces of the HDV, resulting in performance changes associated with tractor modifications being affected more than for trailer modifications. These results represent the first comprehensive study of traffic-wake effects on HDVs at safe inter-vehicle distances in highway-driving conditions, and highlight potential differences in real-world aerodynamic performance relative to the standard wind-averaged uniform-flow metrics used for fuel/energy-use and emissions predictions.

Introduction

Road-vehicle platooning has long been identified as a means to increase traffic density and reduce energy use of road vehicles, with heavy-truck platooning being the concept nearest to commercialization [1, 2, 3, 4]. The energy-saving potential of platooning for highway conditions arise from a combination of improved roadway capacity, with its associated speed harmonization [2], and from aerodynamic interactions between the vehicles that lead to reduced aerodynamic drag [4]. Summaries of the aerodynamic benefits of platooning are provided by Le Good et al. [5] with respect to light-duty vehicles (LDVs) and by McAuliffe and Ahmadi-Baloutaki [6] with respect to heavy-duty vehicles (HDVs). In general, leader and follower vehicles interact aerodynamically and experience changes in drag below about one vehicle-length, while at larger distances only the following vehicle of a given pair experiences an interaction. Some studies have demonstrated drag and fuel-use reductions associated with wake effects of LDVs and HDVs to large distances [7, 8, 9], and suggest that wake effects persist to inter-vehicle distances exceeding 100 m. This coincides with studies of vehicle-wake decay measurements and predictions that show wind-speed deficits persisting far downstream [10, 11, 12], well past 10 vehicle lengths (order of >50 m for LDVs, and > 200 m for HDVs). These distances are much greater than common vehicle spacings encountered on highways. Watkins and Vino [13], using data for the M25 motorway in London, England, show a peak vehicle-separation distance of 6 vehicle lengths (approximately 30 m) with the majority occurring below 12 vehicle lengths (approximately 50-60 m). In a companion paper, McAuliffe and Barber [14] present data from the 400-Series Highways in the Greater Toronto Area, Canada, showing 50 m as the most prevalent separation distance, and with a significant proportion of distances as large as 100 m. Considering the truck-platoon and wake-decay findings with these traffic-spacing characteristics suggests that wake effects

are influencing the aerodynamic performance of vehicles in everyday traffic conditions. Jessing et al. [15] corroborate this hypothesis based on measurements of incident wind-speed in traffic, which showed an average of 14% lower wind speed than the ground speed of the vehicle. Their surface-pressure measurements indicate, based on the similarity of pressure-coefficient values between different traffic scenarios, that the aerodynamic loads on the vehicle are lower when travelling in traffic.

Recognizing that aerodynamic interactions amongst road vehicle are a common occurrence, a project was initiated at the National Research Council Canada (NRC) to examine traffic aerodynamics in a systematic manner. McAuliffe and Barber, in a companion paper [14], document the development of a Road Traffic and Turbulence System (RT^2S) for use with 30%-scale road-vehicle models in the NRC 9mWind Tunnel. They present some preliminary wake-effects results for LDV and HDV models that show measurable drag reductions. The RT^2S is designed to generate wake conditions specific to a range of forward vehicle types, distances, and lane positions, while adapting appropriately for cross-wind/yaw-angle conditions. This paper documents a study to examine the influence of wake effects associated with every-day driving on the aerodynamic performance of HDVs. Ten HDV configurations were tested with up to 53 specific wake/freestream-wind conditions applied to each, for yaw angles up to 11°. The results represent only a tiny subset of the conditions that can be encountered on a roadway, but provide a means to examine specific changes in the aerodynamic performance associated with traffic-wake phenomena.

Experimental Setup

Wind Tunnel

The test program was undertaken in the NRC 9 m Wind Tunnel. The wind tunnel is a horizontal closed circuit atmospheric facility with a large test section (9.1 m wide × 9.1 m high × 22.9 m long) that is suitable for testing tractor-trailer combinations up to full scale. It is powered by an air-cooled 6.7 MW DC motor that provides a maximum wind speed of approximately 55 m/s (200 km/h) in an empty test section. An external mechanical, pyramidal balance senses the six-components of aerodynamic forces and moments.

The test-section configuration used for the current study is shown in Figure 1. A 30%-scale tractor-trailer model is mounted over a 5.6 m × 1.0 m rolling-road system, embedded in the turntable, using streamlined struts connected to the six-component balance under the turntable floor. The Road Turbulence System (see next section) is faintly seen in the photograph of Figure 1 in the upstream settling chamber. Specific to the current tests, and highlighted in the photograph of Figure 1, is a floor-mounted assembly at the inlet of the test section that shrouds the lateral-traverse mechanisms of the wake-generator system, also described in the next section. A boundary-layer suction system is located between the wake-generator assembly and the turntable.

FIGURE 1 Upwind view of the test section with 30%-scale HDV model.

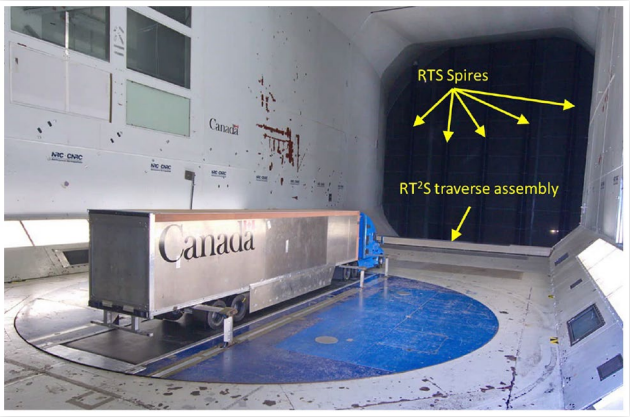

Road Traffic and Turbulence System

The NRC Road Traffic & Turbulence System (RT^2S) is comprised of two systems: the NRC Road Turbulence System (RTS), introduced in 2014; and a traffic-wake-generator system, introduced for this test campaign.

The RTS is a passive turbulence-generating concept using large obstacles mounted in the settling chamber of the wind tunnel, observed faintly in Figure 1. The RTS creates a model-scale terrestrial-wind environment which replicates what an HDV experiences on typical North-American highways. The system provides a turbulence intensity of 4% with turbulence length-scales greater than 1 m, relative to full-scale conditions [16].

The traffic-wake generator system was developed to modify the inlet flow conditions of the wind tunnel to simulate the influence of forward traffic. McAuliffe and Barber [14] document the development of the RT2S, from small-scale concept demonstration through the system used in the current study for testing with 30%-scale road-vehicle models, and show some of the wake flow fields that were simulated.

The wake-generator component of the RT2S consists of grids and sets of up to five vertically-mounted vanes that, when combined in predefined sets of grids and vanes at specific lateral positions and vane yaw angles, creates flow patterns that represent the wakes of specific single-vehicle or traffic conditions in same- or adjacent-lane traffic conditions. The RT2S is shown with an SUV-wake configuration installed in the test section in Figure 2. Target flow conditions used to recreate these specific wake conditions include the size, shape, and locations of the wake, relative to the test model, along with the wind-speed-deficit and flow-deviation-angle distributions within the wakes. These wake characteristics were defined based on a precursor study to investigate the wake of road vehicles [12, 17, 18]. Dynamic motion of the vanes was also introduced, with frequency components between 1 Hz and 30 Hz, to enhance the turbulence in the simulated wake, mainly for regenerating RTS-level turbulence dissipated by the grid/vane combinations and to partially enhance the turbulence to represent conditions in the wakes of road

FIGURE 2 Wake-generator system, part of the NRC Road Traffic & Turbulence System, installed at the inlet of the test section (SUV-wake configuration shown).

vehicles. The vehicle types for which wakes were simulated include:

- CAR: a compact sedan;
- SUV: a mid-sized sport-utility vehicle (SUV);
- HDV: a modern heavy-duty vehicle with sleeper-cab tractor and dry-van trailer; and
- Mixed LDV: a mix of light-duty vehicles (LDVs) including a mid-sized SUV in the same lane and sedans in the left-adjacent lane.

Table 1 provides the specific conditions for which wakes were simulated in the current study.

Test Models

Testing was undertaken with a 30%-scale wind-tunnel model of a heavy duty vehicle (HDV), capable of adopting a range of configurations typical of full-scale HDVs on North American roads.

TABLE 1 Wake-type, effective-distance, effective-lane-location, and yaw-angle (ψ) configurations of the RT^{2}S used for testing.

Wake Type	Vehicle Distance	Same Lane Conditions	Adjacent Lane Conditions
CAR	25 m		ψ = 4.5°, 7.5°, 11°
	50 m	ψ = -2°, 0°, 2°, 4.5°	ψ = -2°, 0°, 2°, 4.5°, 7.5°
SUV	25 m		ψ = -2°, 0°, 2°, 4.5°, 7.5°, 11°
	50 m	ψ = -2°, 0°, 2°, 4.5°	ψ = -2°, 0°, 2°, 4.5°, 7.5°
HDV	50 m	ψ = -2°, 0°, 2°, 4.5°, 7.5°	ψ = -2°, 0°, 2°, 4.5°, 7.5°, 11°
	100 m	ψ = -2°, 0°, 2°, 4.5°	ψ = -2°, 0°, 2°, 4.5°
Mixed LDV	variable	ψ = 0°, 4.5°, 7.5°	

Four primary variants of the tractor-trailer model were tested in the current study, comprised of combinations of three tractor models and two trailer models. Underbody structures of the tractors (fuel tanks, exhaust-system components, mud flaps, etc.) are present with high fidelity in all three versions. The three tractor variants, all of which have a 6x4 axle arrangement, are shown in Figure 3 and described as:

- Day-cab tractor: The initial version of this tractor was modelled after an International ProStar short-sleeper cab from the early 2010's with modifications made to the bumper, hood, A-pillars and roof fairing. The short-sleeper configuration was designed to convert to a smaller day-cab variant, which uses the same components from the driver cab forward, with a different cab-back component and with different interchangeable roofs designed by NRC. Both a high-roof fairing and a low-roof cab are used in the current study.
- Long-sleeper-cab tractor: This tractor model is based on a 3D scan of a model-year 2016 Kenworth T680 high-roof long-sleeper cab. This model represents, to the best of the model-designer's capabilities, the exact external shape of the full-scale vehicle. The wheelbase-adjustable chassis from the short-sleeper model was used as the underlying structure for this model, therefore the engine-bay, suspension, and drive-line components differ somewhat from the scanned vehicle.
- Zero-emission-cab tractor: The adapted-ProStar day-cab tractor was modified to fill in the region above the hood and forward of the windscreen to provide a shallower windscreen angle and large corner radii, similar to geometric characteristics found on emerging battery-electric zero-emission HDV shapes. To simulate the reduced cooling airflow requirements for such vehicles, the large upper front grille was covered, while the lower grille remained open.

The tractor-model chassis, on which all model variants are based, has an engine bay with a representative static engine and its auxiliary components, and uses porous screens to simulate the cooling system for an appropriate level of cooling air flow through the cooling system and engine bay. This internal configuration was used for the zero-emission-cab model as well, despite such emerging vehicle concepts having different internal and underbody configurations. The intent of this configuration was to provide a first-order representation of a zero-emission shape, as an initial step in a separate study examining zero-emission-truck aerodynamics. All tractor-model configurations use an electric-wheel-drive system with treaded-wheel models. The tractor-trailer gap was set to 0.343 m (1.14 m or 45 in full scale) for the current tests.

Two trailer configurations were used during the experiments, also with an electric-wheel-drive system and treaded-wheel models:

- Dry-van trailer: The standard 30%-scale trailer model used for testing in the 9 m Wind Tunnel represents a 53 ft box-van with a tandem-axle wheel setup. The rear trailer axle is positioned 0.91 m from the trailer rear surface (3.05 m full scale). The trailer is modelled after a

FIGURE 3 Photographs of day-cab tractor model (left), sleeper-cab tractor model (middle), and zero-emission-cab tractor model (right).

combination of Wabash and Manac trailers. The standard setup represents a dry-van trailer. The trailer model has many details of a real trailer, including the landing gear, under-body ribs, a rear-impact guard, a drip rail along the upper edges, a rain gutter at the top aft edge, and light- and door-hardware details. Four variants of the dry-van-trailer model were used for testing, with different drag-reduction technologies installed. Figure 4 shows the standard trailer model, without any drag-reduction technologies, while Figure 5 shows the trailer model outfitted with side-skirts and a boat-tail. A configuration with only side-skirts was also tested. A low-drag configuration was also tested, shown in Figure 6 that includes the same side skirts, with a larger boat-tail, and a front fairing. In this low-drag configuration, the tractor-drive- axle and trailer-bogie wheels were replaced by singlewide tires with wheel covers.

FIGURE 4 Standard-trailer model.

FIGURE 5 Trailer model with side-skirts and boat-tail.

FIGURE 6 Low-drag trailer model with side-skirts, large boat-tail, trailer fairing, and single-wide tires with wheel covers. Front-face trailer fairing shown in red in the right photograph.

- Flat-bed trailer: A flat-bed configuration is achieved by removing the upper box from the dry-van-trailer configuration, repositioning the two bogie assemblies, and adding I-beams to the underbody to represent the aerodynamically-obstructive structural elements of a real trailer. This empty flat-bed configuration is shown in Figure 7. An instrumentation box, that typically resides inside the trailer box, is mounted at the forward edge of the bed. A box-cargo configuration was also tested, shown in Figure 8, with five boxes of varying sizes arranged along the length of the bed.

FIGURE 7 Empty flat-bed trailer model.

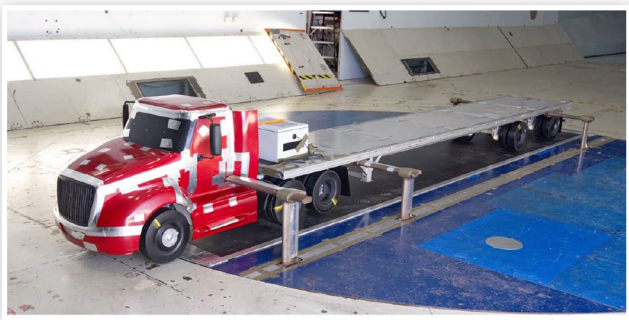

FIGURE 8 Flat-bed trailer model with box cargo.

Instrumentation and Data Processing

Wind-speed and air properties are measured by means of pressure transducers, for the reference dynamic pressure and barometric pressure, and a series of temperature sensors and a humidity sensor in the settling chamber. The dynamic and static pressure in the test section are calculated via a calibration against the reference dynamic pressure and barometric pressure. Air properties (density, viscosity) are calculated using the settling chamber temperature and humidity which, when combined with the calibrated dynamic pressure, are used to calculate the wind speed in the test section.

Force and moment measurements are obtained from an external six-axis pyramidal mechanical balance, mounted below the test-section turntable. From these measurements, tunnel-axis force and moment coefficients are calculated using the test section dynamic pressure and model reference geometry (reference area = trailer width × height, and reference length = model trailer width). The balance-centre-referenced coefficients are then translated to the specified model-moment-centre location, used to calculate and apply wall corrections, and subsequently transformed to a body-axis coordinate system. Strut-tare and strut-interference correction are applied to remove from the calculated coefficients the effect of wind loads imparted to the struts, and to account for the influence of the struts on the model. Adjustments were applied to these strut corrections for the influence of lower-speed flow in the traffic-wake condition, based on estimates from previous wake-flow measurements.

The torque required to maintain wheel speed during testing is measured by the wheel-drive motor/controller system, from which the ventilation-drag coefficient (drag associated with wheel aerodynamic torque) has been calculated and added to the linear drag coefficient. A pre-test procedure is used to quantify the torque requirements to overcome mechanical resistances in the wheel-drive system such that, when subtracted from the measurements, the result is the torque required to overcome rotational aerodynamic loads of the rotating wheels. The inclusion of ventilation drag, which for this model is on the order of 3-4% of the linear drag, provides for this data set a quantification equivalent to the aerodynamic resistance to motion experienced by an HDV on the road.

To provide a single representative measure of the aerodynamic performance of a ground vehicle with which different configurations can be compared, a wind-averaged-drag coefficient (WAC_D) is defined for a given ground speed. The approximation for WAC_D defined by SAE J1252 [19] makes use of the distribution of C_D with yaw angle, combined with a single mean terrestrial wind speed that represents long-term averaged conditions experienced across the United States weighted by the annual truck distance travelled in each state [19]. Recent regulatory procedures by the EPA have simplified the quantification of wind averaging by recognizing a correlation between SAE-method results for 65 mph ground speed and the drag coefficient or drag-area calculated as an averaged of values measured at yaw angles of ±4.5° [20]. Some recent work by the authors has identified quantifiable differences associated with the SAE approach and the EPA approach as compared to the general form of the WAC_D definition (named here the "full-wind" method), specifically for cases with significant asymmetries of C_D with yaw angle which are observed from wake-effects testing. Differences in WAC_D between the methods of up to 0.011 for the SAE method and up to 0.017 for the EPA method, relative to the full-wind method, have been observed for results in the current data set, which is on the order of 2% and 3% of the model wind-averaged-drag coefficient. These general differences were documented by McAuliffe et al. [21]. A more thorough examination of the data presented in this paper, but not all shown, indicates that model-change quantities (ΔWAC_D values) differ by up to 0.005 (about 1%) for the SAE method and up to 0.008 (about 1.5%) for the EPA method. For the current paper, only values using the "full-wind" method are presented.

Surface-pressure measurements were acquired for one of the four primary tractor-trailer variants: the sleeper-cab-tractor with dry-van-trailer model. Pressure measurements were acquired using pressure scanners. One scanner was mounted in the tractor model and two were mounted in the dry-van-trailer model. The model tubing connections were calibrated for their frequency-response characteristics using a combination of a fast-response-pressure-sensor, horn-driver, and spectral-analyser. The frequency- and phase-response characteristics of each pressure-tap tubing line were measured for subsequent correction of the dynamic component of the pressure signals. Mean and root-mean-square surface-pressure coefficients based on these corrected signals have been calculated.

Given the large number of surface-pressure taps installed on the model, taps were grouped into sets for analysis and plotting purposes. Figures 9 and 10 show the pressure taps on the tractor and trailer models, respectively, and identify the sets used for analysis. Each body (tractor or trailer) has a "Centreline" set representing taps along a vertical centreline plane, a "Perimeter" set representing taps along a horizontal plane, and an "Underbody" set representing taps placed at various locations in the lower extremities of the model.

All tractor taps and the "Trailer Underbody and Bogie" taps are identified by a TapID within each set, shown in the figures. The "Trailer Centreline" and "Trailer Perimeter" tap locations are identified by a surface coordinate, s, representing the distance along the surface from a reference location on the front face of the trailer. The "Trailer Centreline" reference

FIGURE 9 Pressure-tap locations for the sleeper-cab-tractor model.

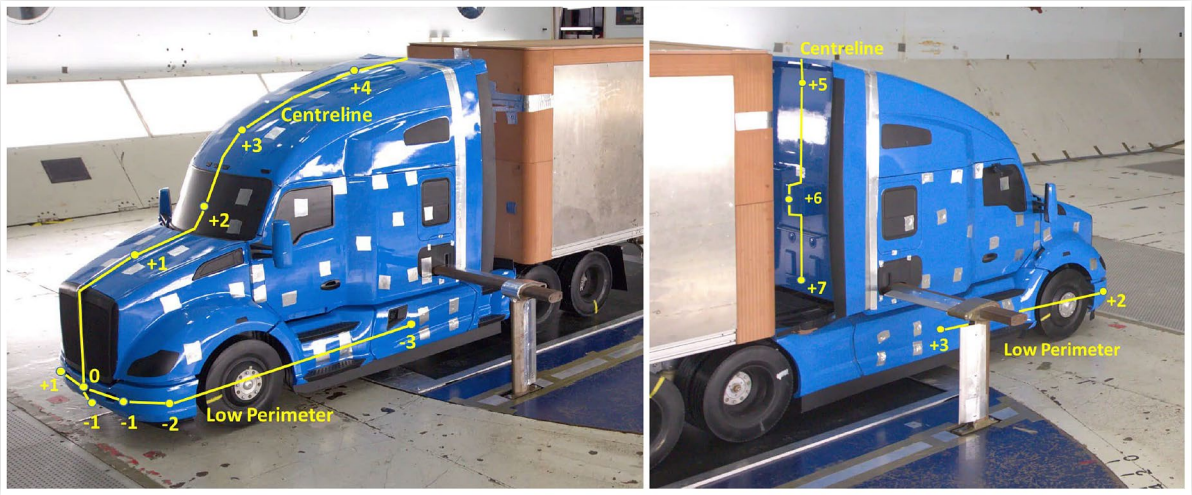

FIGURE 10 Pressure-tap locations for the dry-van-trailer model. Centreline and Midheight Perimeter tap locations are based on surface distance "*s*" with origins identified in upper left image.

s = 0 location is the bottom front edge of the trailer box, with the path of *s* moving up the front face, along the top, and down the base, ending at a tap on the base of the rear-impact guard. The "Trailer Mid-height Perimeter" reference location *s* = 0 is the centreline of the front face, with the path of *s* moving outward along the front face, along the side, and inward along the base to the centre, with negative *s* on the driver side and positive *s* on the passenger side. Photographs of the "Tractor Engine and Underbody" tap locations are not provided, but Table 2 documents the locations from each respective TapID. For the "'Trailer Underbody and Bogie" set of taps, the side-skirt taps (TapIDs ±10, ±11) were only installed for the "Low Drag" model configuration and made use of existing taps and tubing associated with TapID's -5, 0, +1, and +5. Therefore,

data from the the latter tap locations are not available for the "Low Drag" configuration.

Uncertainty magnitudes have been estimated for all measured and calculated parameters. The uncertainty analysis undertaken here is based on the procedures established in Appendix B of the SAE J1252 [19], with an adaptation for calculating the uncertainty of difference values. In the current test program, one model configuration was tested three times over a two day period, providing a data set to calculate the random uncertainty associated with measurement error and repeatability error. The estimated uncertainties for the current test program are provided with the data presented in this paper.

Test Conditions

The test speed used for the current study was 40 m/s, corresponding to a dynamic pressure of about 1000 Pa, a Mach number of 0.12, and a model-width-based Reynolds number of 2.1 million. The Mach number is below 0.25, such that considerations due to compressibility are unnecessary, and the Reynolds number is above one million, as recommended by SAE [19]. In the vicinity of the model, without the RT²S, the gradient of the static-pressure coefficient is small (order of 0.001 m^{-1}). The turbulence generated by the RTS is similar to representative turbulence characteristics experienced by heavy-duty vehicles on Canadian roads, with a turbulence intensity of 4% and a turbulence length scale greater than 1 m [16].

McAuliffe and Barber [14] document many of the wake conditions simulated with the RT²S. Single-vehicle wake sizes, based on a 1% wind-speed-deficit threshold, vary from about the width of the HDV model (CAR and SUV wake) to three times its width (HDV wake), and from about 25% of the HDV-model height (CAR wake) to 150% its height (HDV wake). Peak wind-speed deficits vary between 3% for smaller vehicles at larger distances and 14% for larger vehicles at closer distances. Peak flow-angle deviations within the wakes vary from between 50% to nearly 100% of the freestream yaw angle. This latter conditions represents a local re-alignment of the flow direction with the model longitudinal axis, and is a phenomenon that has been observed in truck-wake measurements on a test track [9].

Aerodynamic Performance in Uniform Flow

Ten tractor-trailer configurations were used for the wake-effects investigations, for which all were tested in uniform-flow conditions. Of these ten configurations, four represent distinct tractor or trailer types, while the remaining are modifications to the respective trailer configuration. These were selected to provide a range of aerodynamic performance and a range of shapes that may show differences from the influence of traffic wakes. The model configurations and associated acronyms are presented in Table 3 with the wind-averaged-drag results for the ten configurations.

TABLE 2 Tractor underbody and engine-bay pressure-tap locations.

TapID	Location Description
-5	Underbody tank (driver side)
-4	Frame rail (driver side)
-3	Front axle (driver side)
-2	Front of engine (low)
-1	Front of engine (high)
0	Front of radiator (high)
+1	Front of radiator (low)
+2	Rear of radiator (ahead of fan screen)
+3	Front axle (passenger side)
+4	Frame rail (passenger side)
+5	Underbody tank (passenger side)

TABLE 3 Model identifier acronyms and wind-averaged drag-coefficient results for the tractor-trailer combinations tested in uniform flow, representing 105 km/h ground speed and 11 km/h terrestrial wind speed. Uncertainties are δWAC_D = ±0.004.

Tractor-trailer Configuration	Trailer Modification	WAC_D [-]
Sleeper-cab with dry-van (SCDV)	Standard (SR)	0.585
	Side skirts (SK)	0.525
	Side-skirts and boat-tail (ST)	0.466
	Low drag (LD)	0.436
Day-cab (high roof) with dry-van (DCDV)	Standard (SR)	0.629
	Side skirts (SK)	0.563
	Side-skirts and boat-tail (ST)	0.499
Zero-emmission-cab with dry-van (ZEDV)	Side skirts (SK)	0.517
Day-cab (low roof) with flat-bed (DCFB)	Empty (EM)	0.465
	Box cargo (BC)	0.737

The wind-load measurements for the ten tractor-trailer combinations in uniform flow are presented in Figure 11. The three force coefficients are presented in the top row of plots and the moment coefficients in the lower row. These plots contain a significant magnitude of data. The intent of its presentation is not to analyse in detail the specific configurations or differences amongst configurations, but to demonstrate the range of HDV aerodynamic configurations and performance to which the RT²S has been applied, forming the baseline conditions for examining wake influences. A few comments are provided in the following to document general performance impacts of the various configurations.

Differences in the drag coefficient amongst the three tractors paired with the dry-van-trailer were discussed in a separate report based on the same set of experiments, specifically examining the potential for the zero-emission-cab shape to provide reduced energy use over the conventional shapes [21]. That report demonstrated that the sleeper-cab-tractor configuration exhibits lower aerodynamic drag than the day-cab, and showed that the conversion of the day-cab shape to represent emerging zero-emission-cab shapes reduced the

FIGURE 11 Force-coefficient measurements for the ten tractor-trailer configurations in uniform flow. The measurement confidence interval is of the size of the symbols or smaller.

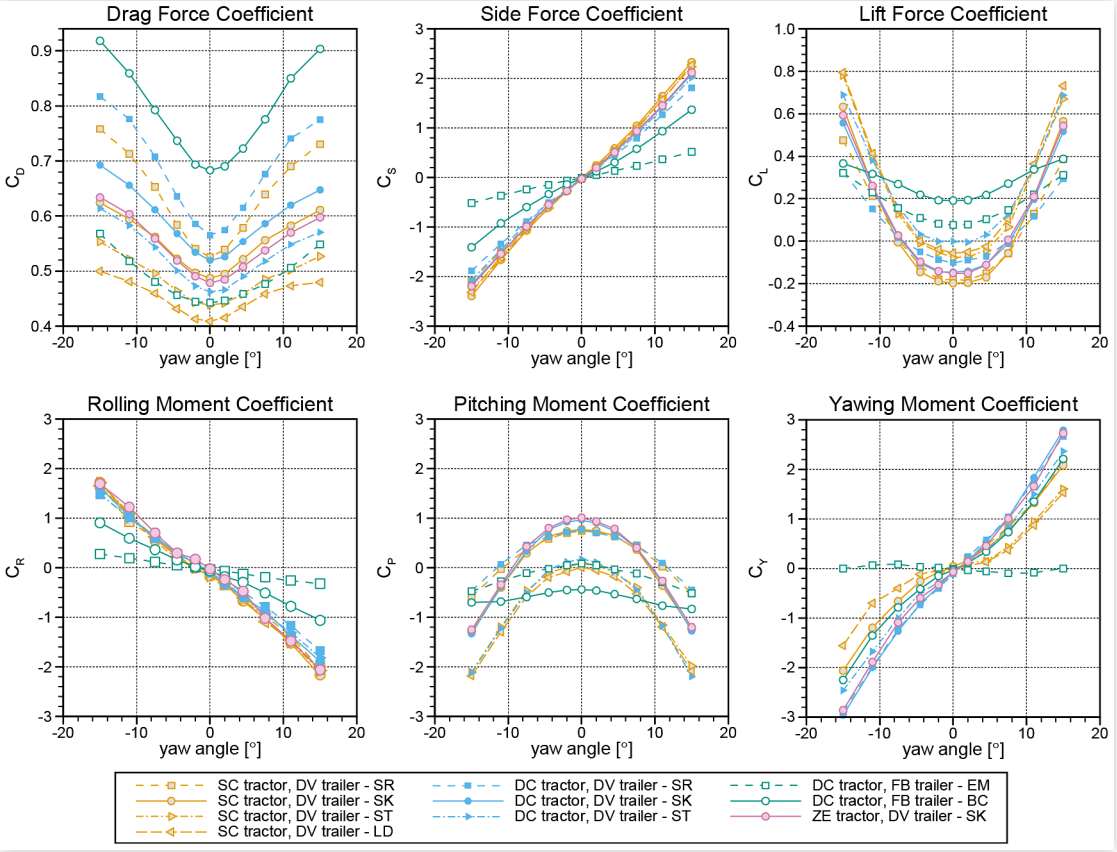

aerodynamic drag-area of the vehicle by 7-9%, bringing the drag down to a level similar to the sleeper-cab tractor.

The dry-van-trailer (DV) drag-coefficient results of Figure 11 show increasing levels of drag reduction when incremental aerodynamic technologies are installed on the model. The side-skirts and boat-tail each provide drag reductions of comparable magnitude, with the side-skirt improvements demonstrating greater sensitivity to yaw angle than the boat-tail improvements, as has been observed in other studies ([22, 23]). These observations are consistent between the sleeper-cab and day-cab tractor configurations. Other observations for these dry-van-trailer data, with respect to the drag-reduction technologies, include:

- The side-force coefficient is influenced mainly by side-skirts, with approximately 10% increase in magnitude when skirts are installed. This is caused by a greater side area of the model with side skirts, blocking air from entering the under-body in cross-wind conditions. The rolling-moment coefficient shows signs of the same effects from side-skirts but the high uncertainty magnitude precludes the confirmation of this finding.
- The lift-force, pitching-moment, and yawing-moment coefficients all demonstrate the most sensitivity to the installation of a boat-tail, with higher lift force and lower moments when installed. The changes in lift force and pitching moment are due to the suction created near the upper rear edge of the trailer from the boat-tail, which directs the flow in a curved downward trajectory, resulting in an upward force at the rear (increased lift force and reduced nose-down pitching moment). These two parameters show some sensitivity to side-skirts at higher yaw angles, above about ±10°, likely due to changes in the pressure field surrounding the trailer bogie.
- The additional drag-reduction technologies for the LD configuration (trailer front fairing, larger boat-tail, wheel covers and single-wide tires) primarily influence the drag-force coefficient, with little to no effect on the other forces and moments.

The most significant changes to the overall wind loads on the truck model arise from the major reconfiguration to a low-roof day-cab-tractor and flat-bed-trailer model. Despite having a lower roof height, for the empty-trailer setup, the coefficient values have been calculated with the same frontal area as the high-roof configurations, to permit direct comparison of the overall wind-load magnitudes, analogous to a C_DA comparison. The empty-flat-bed configuration exhibits lower magnitudes of the wind-load coefficients and lower sensitivity of these parameters to yaw-angle, resulting from the smaller frontal and side areas of the model. When adding box cargo, the drag-force coefficient increases significantly, well beyond the magnitude of the zero-emission- cab with dry-van measurements, while the moment coefficients increase marginally but not to the levels measured for the

dry-van-trailer configurations. Increased drag is mainly due to the exposure of the large sharp-edged boxes that are not shielded by a tractor roof fairing. The reduction in other parameters is principally due to the smaller surface areas of the cargo boxes compared to the large dry-van box.

To provide a quantitative comparison of the aerodynamic drag for the various tractor and trailer configurations, Table 3 lists the wind-averaged drag coefficient results for all ten uniform-flow test configurations of interest to the current study. The wind-averaged-drag-coefficient values show a large range, from 0.436 for the sleeper-cab tractor with the low-drag dry-van trailer, to 0.737 for the low-roof-day-cab tractor with the flat-bed-with-box-cargo trailer, providing a variety of sources of drag production (or savings) for the subsequent evaluation of wake effects.

Only one of the four principal HDV configurations, the sleeper-cab tractor with dry-van trailer (SCDV) configuration, was instrumented with surface pressure taps during the experiments. These measurements provide a means to examine the source of wind-load changes of the HDV model associated with the different flow conditions. A sample of the surface-pressure measurements are provided in Figures 12–14. Each figure represents a different yaw angle (0°, 4.5°, and 7.5°), with each showing pressure-coefficient results for the four variants of the SCDV model. In each figure, the upper row of plots show measurements from the tractor model with the lower row showing trailer results, while each column represents specific sets of measurements (vertical centreline, horizontal perimeter, and underbody). The pressure-tap locations were documented in Figures 9 and 10 and in Table 2. Each plot shows the mean pressure coefficient C_P with the associated scale on the left axis, and the rms pressure coefficient C_{Prms} with scale on the right axis.

An immediate observation for all three yaw angles is the negligible difference in mean and rms pressure coefficients for the tractor (upper row) amongst the four HDV configurations, within the respective uncertainty magnitudes. This result was expected, given that the tractor model is not altered amongst the four variants. The tractor-centreline measurements show similar trends at all three yaw angles, with high positive C_P values on the front bumper and wind shield, indicating stagnation or near-stagnation conditions. The under-bumper and hood taps show near-zero or positive C_P, while the roof fairing and gap region show negative C_P values resulting from the displaced and accelerated air adjacent to the top and sides of the model, with the gap-region-pressure equalizing with the surroundings at a C_P of about -0.2. The C_{Prms} results show elevated values on the forward surfaces, compared to the gap region, which indicates that the flow in the gap region is relatively stagnant without much turbulence compared to the surrounding road-representative turbulent flow.

The tractor-low-perimeter results at 0° yaw angle in Figure 12 demonstrate the transition from stagnating flow near the bumper centre (large positive C_P values for tap IDs -1, 0, +1) to strong acceleration around the front corners (large

FIGURE 12 Pressure-coefficient measurements for the sleeper-cab-tractor model (SC) paired with the dry-van-trailer model (DV) for all four variants in uniform flow at a yaw angle of 0°. Measurement uncertainty is of the size of the symbols or smaller for the C_P values (approximately ±0.04) and double the symbol size for the C_{Prms} values (approximately ±0.01).

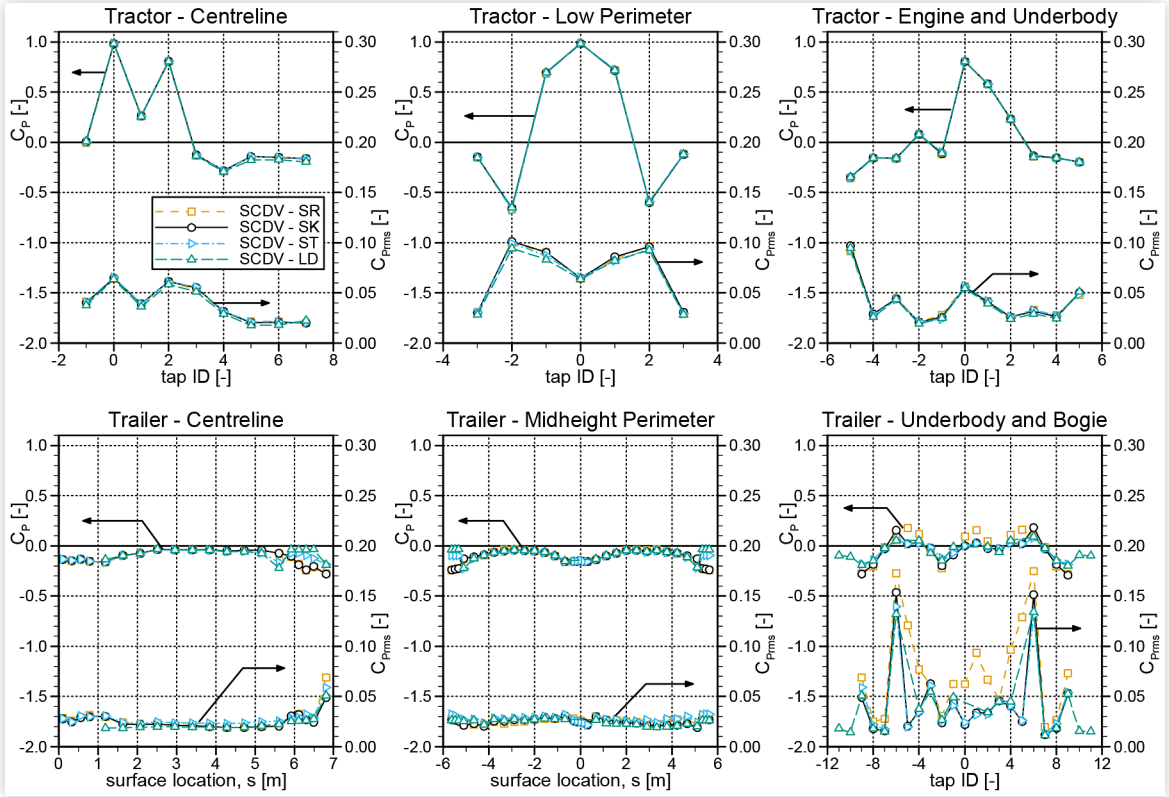

FIGURE 13 Pressure-coefficient measurements for the sleeper-cab-tractor model (SC) paired with the dry-van-trailer model (DV) for all four variants in uniform flow at a yaw angle of 4.5°. Measurement uncertainty is of the size of the symbols or smaller for the C_P values (approximately ±0.04) and double the symbol size for the C_{Prms} values (approximately ±0.01).

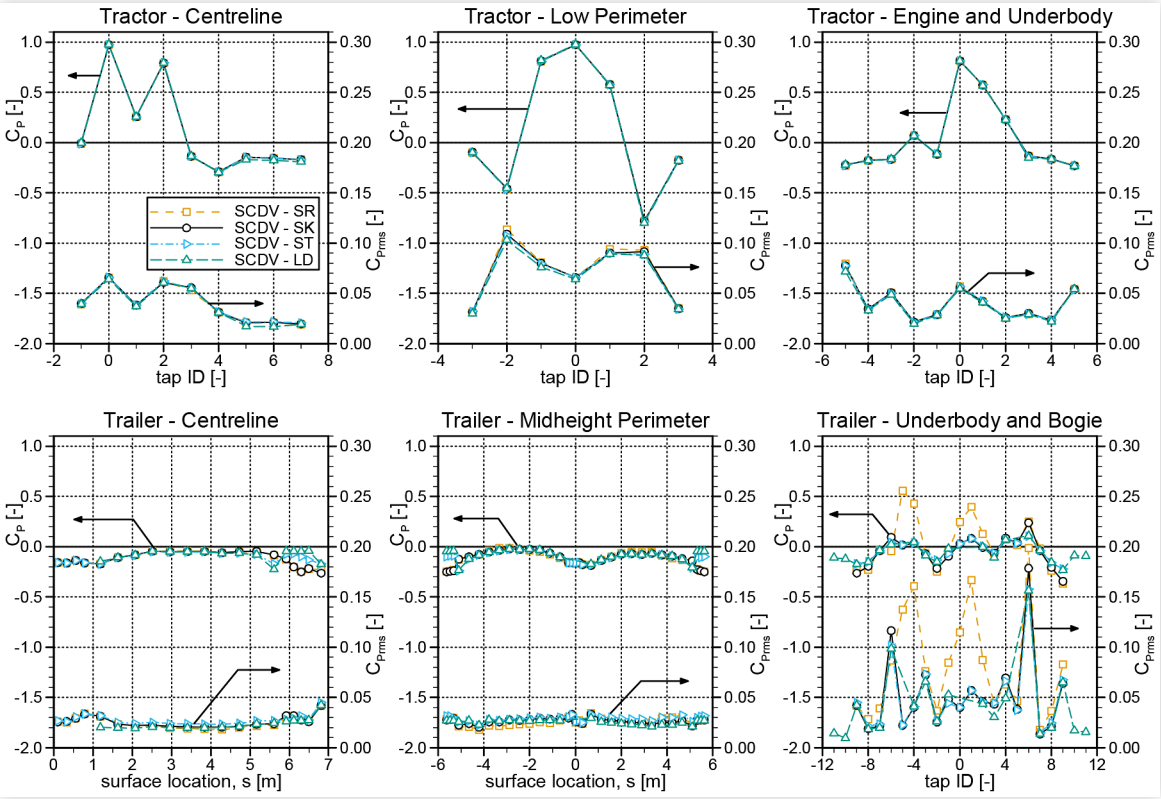

FIGURE 14 Pressure-coefficient measurements for the sleeper-cab-tractor model (SC) paired with the dry-van-trailer model (DV) for all four variants in uniform flow at a yaw angle of 7.5°. Measurement uncertainty is of the size of the symbols or smaller for the C_P values (approximately ±0.04) and double the symbol size for the C_{Prms} values (approximately ±0.01).

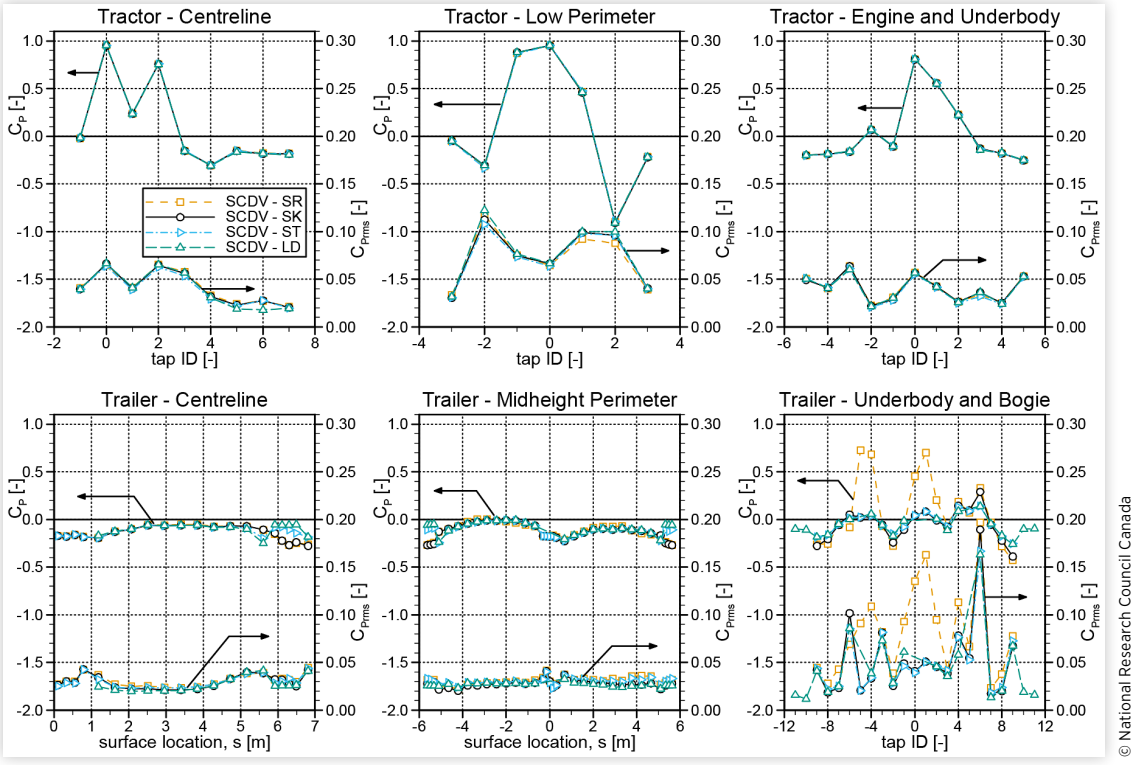

negative C_P values for tap IDs -2 and +2) and stabilization along the sides (tap IDs -3, +3). Peak C_{Prms} values for the tractor occur at the highest-acceleration regions around the front corners (tap IDs - 2 and +2). As the yaw angle is increased (Figures 13 and 14) the C_P results show a movement of the stagnation region associated with the redirection of the freestream flow (peak C_P moves toward -ve tap IDs), with peak acceleration (negative C_P) occurring on the leeward front corner. At yaw, the highest C_{Prms} values remain around the front corners.

In the tractor engine-bay and underbody region, there is limited influence of yaw angle on the pressure field. Tap IDs 0 and +1 show stagnation on the front surface of the simulated radiator with taps +2, -1 and -2 being stagnation regions past the cooling system, showing much lower C_P values due to the pressure loss across the simulated radiator system. The remainder of the underbody taps, except tap ID -5, show C_P values between about -0.3 and -0.1. Tap ID -5, located on the underbody surface shows the highest sensitivity to yaw angle of these taps with the lowest C_P and highest C_{Prms} values at 0° yaw angle, suggesting there may be locally-strong winds in its vicinity, compared to the other underbody and engine-bay taps.

The trailer surface pressures demonstrate a greater influence of HDV configuration than do the tractor surface pressures, particularly in the base and underbody regions. The largest differences are observed for the skirts-removed (SR) configuration that shows significant differences in the underbody and bogie pressures, compared to the other three configurations. Without side-skirts, higher-speed flow entrained from the surroundings impinges on the front surfaces of the trailer bogie (tap IDs -5, -4, 0, +1, +2, +4, +5), with differences in C_P and C_{Prms} more pronounced at yaw. Peak C_P and C_{Prms} values for the configurations with side skirts (SK, ST, LD) are observed at the outboard rear-impact-guard front surface which is exposed to the flow entrained inboard downstream of the wheels and mud flaps, particularly on the windward side at yaw (positive tap IDs).

The trailer centreline and midheight-perimeter results show similar characteristics along the length of the trailer, with differences observed primarily at the base of the trailer. Along the sides of the trailer (for s from about 0.9 m to 5.7 m for the centreline and from ±0.4 m to ±4.8 m for the perimeter) C_P is most negative at the forward and aft ends (between -0.20 and -0.15) with a maximum along the middle section (between -0.05 and 0). For the SR and SK configurations, without boat-tails, the minimum C_P values occur on the base surface (between -0.3 and -0.2). With a boat-tail installed the base pressure is increased, which contributes to its drag-reduction benefit. The large boat-tail used for the LD configuration provides greater base-pressure increase than the smaller tail used for the ST configuration. C_{Prms} values remain low over the top and side surfaces of the trailer, with only the tap on the base of the rear impact guard showing values exceeding 0.04. Tap IDs ±10 and ±11 for the LD configuration in the underbody and bogie plots are taps added to the sides of the side-skirts for those specific tests, which show similar C_P and C_{Prms} values as the sides of the trailer.

The C_{Prms} values provide some indication that the HDV body acts to reduce some of the freestream turbulence in its vicinity. The highest-C_{Prms} values are observed on the forward-oriented surfaces that are exposed to the freestream wind and its elevated fluctuating velocity components. As the flow deviates from the freestream direction to follow the vehicle body, it is presumed that the reduced C_{Prms} values are a result of less fluctuations in the flow due to the obstruction by the vehicle body, which acts to damp a component of the turbulence perpendicular to the local body surface.

Influence of Wake Effects on Force and Moment Coefficients

The test program included a large range of traffic-wake conditions (see Table 1) applied to a large number of HDV configurations, providing a complex set of data with which to evaluate the influence of wakes. To simplify the presentation of results and discussion, the influence of wake effects on a single HDV configuration is documented first, with the secondary influence of HDV configuration examined in the next section.

Although the primary focus of the current work is the influence of traffic wakes on the aerodynamic drag of an HDV, which relates directly to energy use and greenhouse-gas emissions, it is also worth examining the influence of wakes on all the force and moment coefficients experienced by an HDV given their potential importance to handling and stability. Figure 15 presents the wake-effects results for all six coefficient parameters for the sleeper-cab-tractor with skirts-outfitted dry-van trailer (SCDV-SK) with wake-source vehicles effectively in the same lane, while Figure 16 presents the corresponding results for the cases with wake-source vehicles effectively in an adjacent lane. The "Mixed LDV" wake case is repeated in both figures since it represents a condition with LDVs in multiple lanes.

In Figures 15 and 16, the line and symbol style/colour systematically represent differences in the wake-source vehicles and their effective distances. Black solid lines and circles represent the uniform-flow data presented in the previous section. Colour and line style differentiate wake-source-vehicle types, while symbol shape and fill style represent effective distance. The size of the symbols represent the uncertainty range of the respective measurements, which is about ±0.8% for the drag coefficient values.

Some reference to surface-pressure results are provided in the following discussions, without explicitly showing such results, but with reference to the uniform-flow results of the previous section. Surface-pressure-coefficient measurements in wake flows are presented after the force- and moment-coefficient measurements.

Given that the SUV-wake case shares characteristics with the CAR and HDV wakes, and is a component of the Mixed-LDV-wake case, its influence on the HDV aerodynamic forces and moments is described first, followed by the other vehicle-wake conditions.

FIGURE 15 Force-coefficient measurements for the sleeper-cab-tractor model paired with the dry-van-trailer model with side-skirts (SCDV-SK) in same-lane-vehicle wake flows. Measurement uncertainty is of the size of the symbols or smaller.

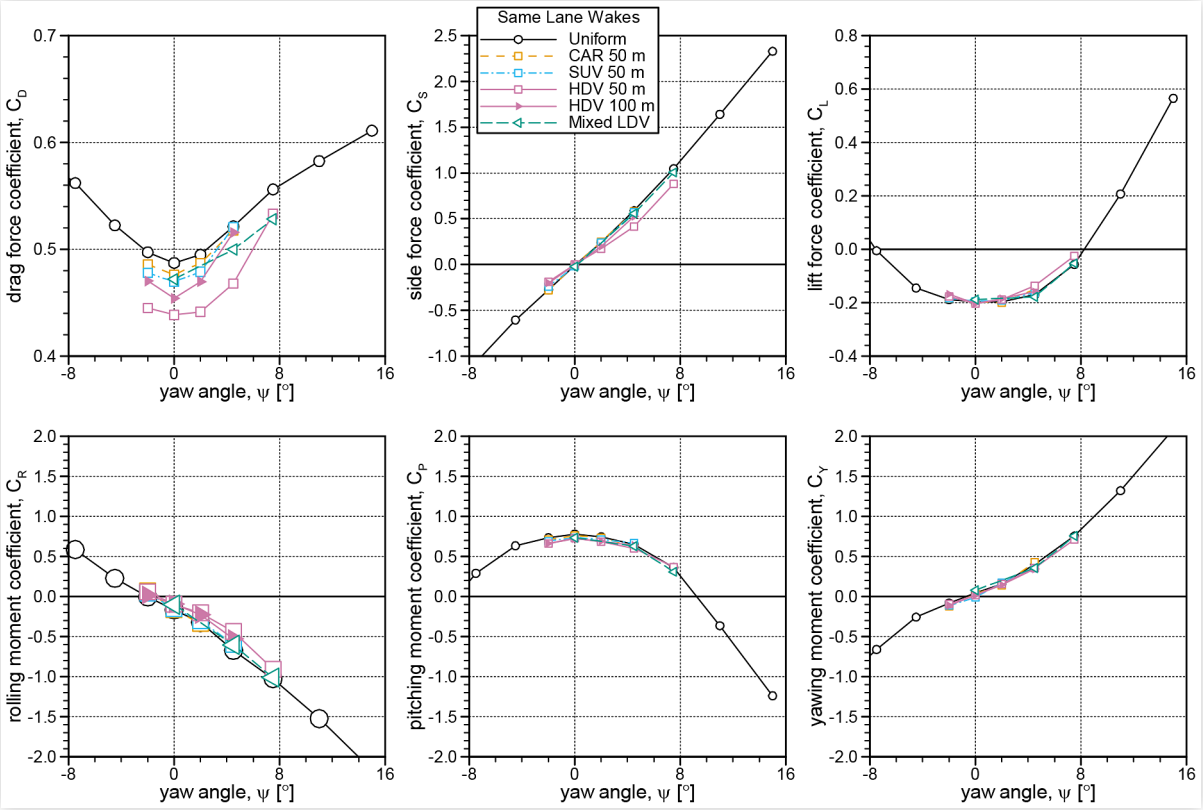

FIGURE 16 Force-coefficient measurements for the sleeper-cab-tractor model paired with the dry-van-trailer model with side-skirts (SCDV-SK) in adjacent-lane-vehicle wake flows. Measurement uncertainty is of the size of the symbols or smaller.

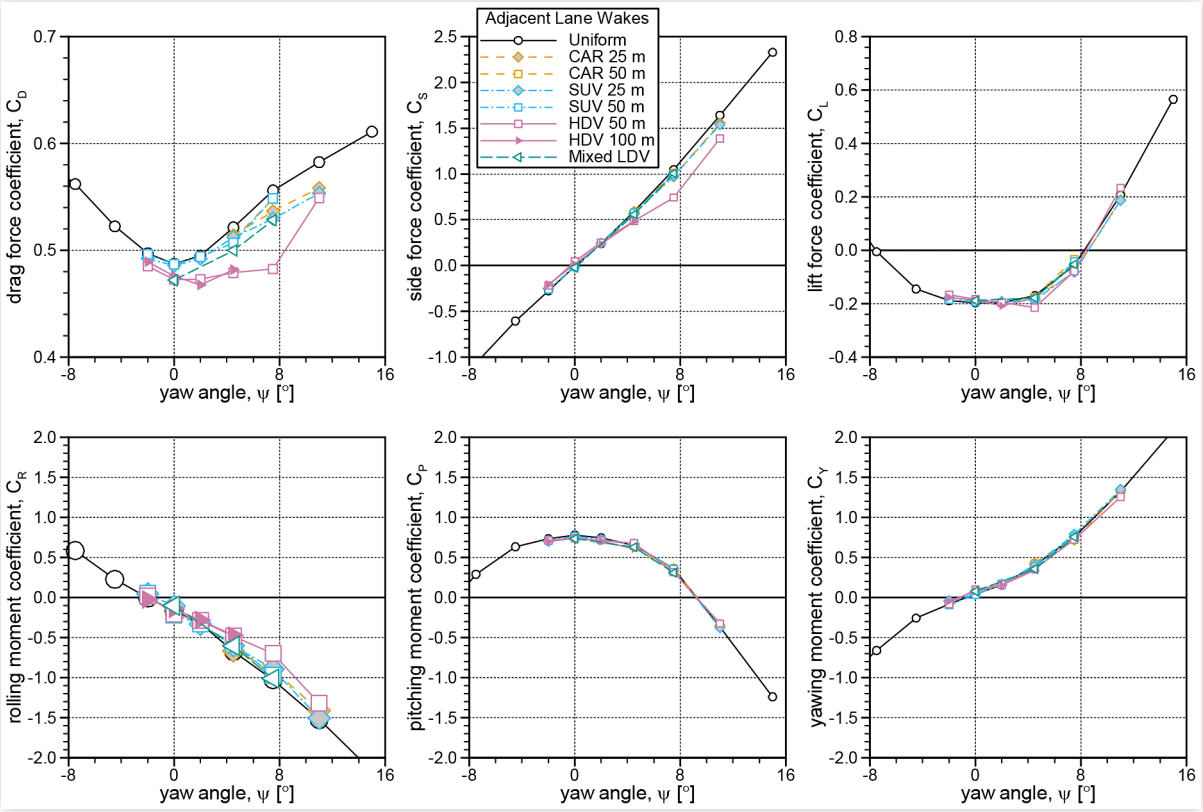

SUV-Wake Influence

Three SUV-wake conditions have been tested, with 50 m same-lane, 50 m adjacent-lane, and 25 m adjacent-lane conditions, each under a range of yaw angles from -2° up to 4.5°, 7.5°, or 11°, respectively.

With an SUV in the same lane (Figure 15), at 50meffective distance, a reduction in HDV drag coefficient was observed only at yaw angles of -2°, 0°, and 2°, with no influence measured at the highest tested yaw angle of 4.5°. At each of these lowest three yaw angles, the drag-coefficient reduction is about 3-4%. The SUV wakes at the low yaw angles cover an area as high as, and wider than, the HDV model, with peak wind-speed deficits of about 4-5% (not shown here, but simulated wakes are described by McAuliffe and Barber [14]). At higher yaw angles the same-lane SUV wakes are convected to the side of the HDV.

For the SUV in an adjacent lane (Figure 16), the yaw angles at which wind-loads of the HDV are influenced change. No measurable influence is observed at -2°, 0°, and 2° for the 25 m or 50 m distances. This is a result of the SUV wakes residing in the adjacent lane for these conditions and not impinging on the HDV model. At 4.5° and 7.5° angles, a 2% and 1% reduction in C_D are observed, respectively, for the 50 m distance case. Partial coverage of the SUV wake over the HDV-model frontal area occurs for these two cases, with corresponding changes in tractor C_P values (shown later). At the closer effective distance of 25 m, for which a larger wind-speed-deficit peak up to 9% was measured in the wake flow, reductions in C_D are 1%, 5% and 5% at yaw angles of 4.5°, 7.5° and 11°. The trend in movement of the maximum influence to larger yaw angles, as the effective vehicle distance is reduced, is a result of reduced lateral shift of the wake at close distances, which requires a greater cross-wind magnitude (yaw angle) to push the wake towards the HDV in the adjacent lane.

With respect to the other forces and moments, only the highest-yaw-angle adjacent-lane wake conditions have a measurable influence, and only on the side-force coefficient. A reduction in side-force coefficient up to 7% is observed, which is a greater relative magnitude than what is observed for drag reduction. This provides some evidence that wind-speed deficit is not the only effect on the aerodynamic loads. As described by McAuliffe and Barber [14], the yaw angle of the flow is reduced, relative to the HDV, in the lower section of the wakes under yaw conditions. For example, at 11° yaw angle, the peak lateral flow angle near the ground is around 6° thus the effective yaw angle at that location is only about 5°. This suggests that the HDV aerodynamic performance is operating at a lower effective yaw angle in wake-flow conditions.

CAR-Wake Influence

As documented by McAuliffe and Barber [14], the CAR-wake cases are the weakest of all the simulated wakes in this study. As a result, they generally have the smallest influence on the HDV model. Except for a small number of conditions noted in the following, there was no measurable influence of the CAR wakes on the side- and-lift-force coefficients, nor on any of the moment coefficients. Only the drag coefficient demonstrated sensitivity to the CAR wakes greater than the experimental uncertainty.

With a CAR in the same lane at 50 m distance (Figure 15), the trend is the same as with an SUV in the same lane. A reduction in HDV drag coefficient was observed only at yaw angles between ±2°, with a drag-coefficient reduction of about 2% at all three tested yaw angles in this range, which is smaller than the 3-4% observed for the SUV wake under these conditions.

For the CAR in an adjacent lane (Figure 16), again the trends are similar to the corresponding SUV-wake cases. At 50 m effective distance, the drag reductions from the CAR wake are the same as those for the SUV wake (1% and 2% for yaw angles of 4.5° and 7.5°), despite there being different exposure areas of the wind-speed deficit patterns. At 25 m distance, smaller drag reductions are observed at 7.5° and 11° yaw angles (3% and 4%) than the corresponding SUV cases (5% each), as might be expected. Given the C_D uncertainty magnitude of ±0.8%, some of the same-versus-different trends may be influenced by the uncertainty bounds of the experimental data. However, these results provide clear evidence that the HDV model experiences reduced aerodynamic drag when exposed to wakes representing a compact sedan at safe following distances or in an adjacent lane.

Mixed-LDV-Wake Influence

The Mixed-LDV wake conditions were an attempt to develop flow characteristics similar to a traffic-scenario used during a truck-platooning investigation on a test track, for which a single HDV followed a two-lane three-vehicle traffic pattern [9]. However, limitations in the grid and vane arrangement of the RT^{2}S generated lower wind speed deficit patterns for the Mixed-LDV configuration compared to what was observed on the track with grille-mounted vane anemometers. The Mixed-LDV results that are repeated between Figures 15 and 16 show drag reductions of 3%, 4% and 5% at yaw angles of 0°, 4.5°, and 7.5°, respectively, which are considerably lower than the track-measurements results of 9±3%, even when considering the experimental uncertainty of the wind-tunnel measurements (±0.8%). Front-grille flow-rate measurements from the track data, measured approximately 1 m from the ground, show greater deficits (10%, [24]) than the wind-speed deficits measured in the wind tunnel at the same corresponding height (3-4% [14]).

Of particular note here is the influence of the Mixed-LDV wake conditions over a larger range of yaw angles than observed from the individual-wake CAR or SUV conditions, which suggests that drag reductions associated with general multilane traffic effects may be less sensitive to yaw angle than are individual-vehicle-wake or single-lane-traffic conditions.

The Mixed LDV results do not show any measurable influence of this traffic scenario on the other force and moment coefficients for the range of yaw angles examined.

HDV-Wake Influence

The HDV wake cases have the largest influence on the HDV-model forces and moments, both for same-lane (Figure

15) and adjacent-lane (Figure 16) conditions. The same-lane HDV scenario is essentially a truck-platooning configuration, although the effective distances (50 m and 100 m) represent conditions for which vehicle-to-vehicle automation is not necessarily required for safety. Only a few truck-platooning aerodynamic studies have examined distances this large, with [25] presenting fuel-economy measurements up to 87 m, [9] presenting track-based drag-area measurements for distances up to 78 m, and [8] presenting wind-averaged-drag-coefficient data from wind-tunnel experiments up to an equivalent of 97 m. Those studies suggest that drag reductions in excess of 10% may be experienced at 50 m inter-vehicle distance, and drag reductions of 5% or more being possible at about 100 m.

At zero yaw angle, the same-lane data in Figure 15 shows 10% C_D reduction for 50 m distance, and 7% reduction at 100 m, which is consistent with the findings of others noted above. As yaw angle increases, the benefits from the 100 m distance decrease at a greater rate, with negligible benefit measured at 4.5°, than the 50 m case which shows about 10% benefit up to 4.5° yaw angle, and 4% at 7.5°. This increased sensitivity to distance is caused by the wake of a further vehicle being convected a greater lateral distance for a given yaw angle, thus impacting the HDV model over a smaller range of yaw angles.

For adjacent-lane conditions (Figure 16), both the 50 m and 100 m distances show similar C_D reductions (within 1%) at all yaw angles for which the 100 m case was simulated, between -2° and 4.5°. Here, greater drag reductions are observed at off-zero yaw angles, consistent with the CAR and SUV adjacent-lane conditions, resulting from the wake convecting from the adjacent lane. The 50 m adjacent-lane case shows the largest drag reduction of all measured cases for this HDV model, with 13% C_D reduction at 7.5° yaw angle. Flow measurements presented by McAuliffe and Barber [14] show, for this condition, the wake nearly centered on the HDV model with a strong wind-speed deficit (15% near the ground) and a significant side-wash that may be effectively reducing the yaw angle over the lower half of the HDV model (about 0.5° yaw angle near the ground, resulting from the 7° peak lateral flow angle). This effective reduction in yaw angle is also implied by the significant reduction in the magnitude of side-force and rolling-moment coefficients at the higher yaw angles. However, the pitching-moment, yawing-moment, and lift-force coefficients do not show significant changes that would imply reduced yaw angles. These observations suggest that the wake flows affect the HDV model in a localized manner and not strictly as an effective change or re-scaling of the oncoming flow field.

Influence of Wake Effects on Wind Averaged Drag Coefficients

To provide some context for how these wake conditions apply in a wind-averaged sense, Table 4 provides the calculated wind-averaged drag-coefficient values for the SCDV-SK model

TABLE 4 Wind-averaged drag-coefficient results for the sleeper-cab-tractor model paired with the dry-van-trailer model with side-skirts (SCDV-SK) in wake flows. Uncertainties are $\delta\Delta WAC_D$ = ±0.003 (±0.6%).

	Same Lane Wakes		Adjacent Lane Wakes	
Flow Condition	WAC_D [-]	ΔWAC_D [%]	WAC_D [-]	ΔWAC_D [%]
Uniform	0.525	-	0.525	-
CAR 25 m			0.522	-0.6%
CAR 50 m	0.520	-1.1%	0.523	-0.4%
SUV 25 m			0.520	-1.1%
SUV 50 m	0.516	-1.7%	0.522	-0.6%
HDV 50 m	0.481	-8.5%	0.504	-4.0%
HDV 100 m	0.510	-2.9%	0.512	-2.6%
Mixed LDV	0.514	-2.1%	0.514	-2.1%

configuration, and the associated percentage reductions compared to uniform conditions, for each of the wake conditions. Although data were not acquired over the full-range of requisite yaw angles for each wake condition, some assumptions have been made to provide C_D values over the full range of yaw angles from -15° to +15° to permit the use of the Full-wind calculation method that was previously found to be more accurate for yaw-asymmetric data. For most of the flow conditions, the uniform-flow C_D data was substituted for any yaw-angle condition not directly measured, with the following exceptions:

- HDV 50 m same-lane condition: at yaw angles of -7.5° and -4.5°, the difference in C_D between the wake-flow results and the uniform-flow results at the corresponding positive yaw angles were used to adjust the uniform-flow results, assuming yaw-symmetric wake effects at these yaw-angle magnitudes.
- Mixed LDV condition: at a yaw angle of +2°, the average difference between wake- and uniform-flow results at 0° and +4.5° was used to adjust the uniform-flow value, otherwise the uniform-flow value was used at all other yaw angles (all negative yaw angles, and all those above 7.5°).

Given the trends in the C_D data with yaw angle, these assumptions should provide reasonable estimates for the full C_D distributions with yaw angle, at least for the purpose intended here which is to examine approximate relative differences associated with the selected wake-flow conditions.

The largest wind-averaged drag reductions are for the HDV wakes, with nearly 9% reduction observed for same-lane conditions and 4% for adjacent-lane conditions. The large-distance results provide additional evidence to support the argument that wake effects are the reason why track-based platooning studies have shown measurable fuel savings at large inter-vehicle distances, up to 87 m [25, 26, 24].

The wind-averaged-drag-coefficient results of Table 4 should not be used to make conclusions about traffic effects in general. A greater consideration of expected traffic conditions on the road is required to do so. These results are strictly an indicator of the influence of wake effects for the particular scenarios tested. The important take-away from these wind-averaged results is that measurable reductions in the

aerodynamic drag of a heavy-duty vehicle, even in long-term averaged conditions, are experienced for vehicles that regularly travel in traffic, even for safe inter-vehicle distances.

Influence of Wake Effects on Surface Pressure Coefficients

As highlighted by McAuliffe and Barber [14], the surface-pressure-coefficient data are suitable for examining the source of changes in the wind loads of the HDV model when exposed to traffic-wake flow fields. Again, only results from the skirts-outfitted configuration (SCDV-SK) are presented to highlight the important findings with respect to wake-effects, with the wake influence towards different HDV configurations discussed later.

Figures 17 and 18 show the wake-effect influence on tractor surface-pressure coefficients for the SCDV-SK configuration at yaw angles of 0° and 4.5° for same-lane wake conditions, with Figures 19 and 20 showing the results at yaw angles of 0° and 7.5° for adjacent-lane wake conditions. The plots in each figure represents specific sets of tractor-specific measurements (vertical centreline, horizontal perimeter, and underbody), similar to the top row of Figures 12 through 14. The pressure-tap distributions were documented in Figures 9 and 10 and Table 2. Rather than showing the mean pressure coefficient, as was done for the uniform-flow results of Figures 12 through 14, these plots show the change in mean pressure coefficient relative to the uniform-flow results ΔC_P, which highlights better the wake effects, in addition to the rms pressure coefficient results C_{Prms}. The ΔC_P results are associated with the scale on the left axis, and the C_{Prms} with scale on the right axis.

For same-lane conditions at 0° yaw angle (Figure 17), all wake-flow conditions tested have an influence on the pressures over the front surfaces of the tractor model. In general, the ΔC_P values are negative for positive uniform-flow C_P values, and positive for negative uniform-flow C_P values, indicating a general reduction in C_P magnitude relative to $C_P = 0$. This is consistent with the overall reduction in local dynamic pressure associated with the wake flows. The CAR 50 m case shows the smallest influence, affecting only the lower front surfaces (centreline tap ID 0, low-perimeter taps IDs -2 through +2, and engine-bay taps 0, +1 and +2), consistent with the small vertical extent of the wake (about 25% to 50% of HDV model height). For taller wakes (SUV, HDV, and Mixed LDV cases), the centreline C_P values show a greater vertical influence of the wakes, with the HDV case affecting all external tap locations (up to tap ID 4). Pressures in the gap region (Tractor-Centreline tap IDs 5 through 7, and Trailer-Centreline locations below 0.9 m) do not appear to be measurably-influenced by the wakes. The trend in stagnation-region C_P changes corresponds with trends observed in the drag-coefficient results of Figure 15. The unsteady pressures (C_{Prms}) show similar or increased magnitudes in Figure 17 for all but the Mixed LDV case, which is a case for which the turbulence of the wake flows was not simulated well due limitations of vane positioning relative to the grid.

For the same-lane conditions at 4.5° yaw angle (Figure 18), only two of the wake cases (HDV 50 m and Mixed LDV) show measurable changes to the tractor surface-pressure coefficients. This is consistent with the C_D measurements of Figure 15. For these cases, the low-perimeter ΔC_P distributions show lateral asymmetry, which is indicative of either lateral shear across the front surface or a change in effective yaw angle. The flow fields of each of these cases (not shown here) demonstrate lateral shear and reduced flow angularity near the ground, but the shear is of opposing signs. The HDV 50 m case has reducing wind speed from left to right at the low-perimeter tap height (0.16 m from ground, approx. 0.5 m full scale), while the Mixed LDV case has increasing wind speed from left to right at this height. This opposing trend in lateral shear suggests that the lateral asymmetry in C_P distribution, that is similar for each of these cases but with differing magnitude, is likely dominated more so by an effective reduction in yaw angle of the bulk flow over the front surfaces of the HDV, with a less significant influence from the lateral shear.

FIGURE 17 Tractor surface-pressure-coefficient measurements for the SCDV-SK configuration in same-lane-vehicle wake flows at 0° yaw angle. ΔC_P is relative to uniform-flow at the same yaw angle (those results found in Figure 12). Measurement uncertainty is of the size of the symbols or smaller for the C_P values (approximately ±0.02) and double the symbol size for the C_{Prms} values (approximately ±0.01).

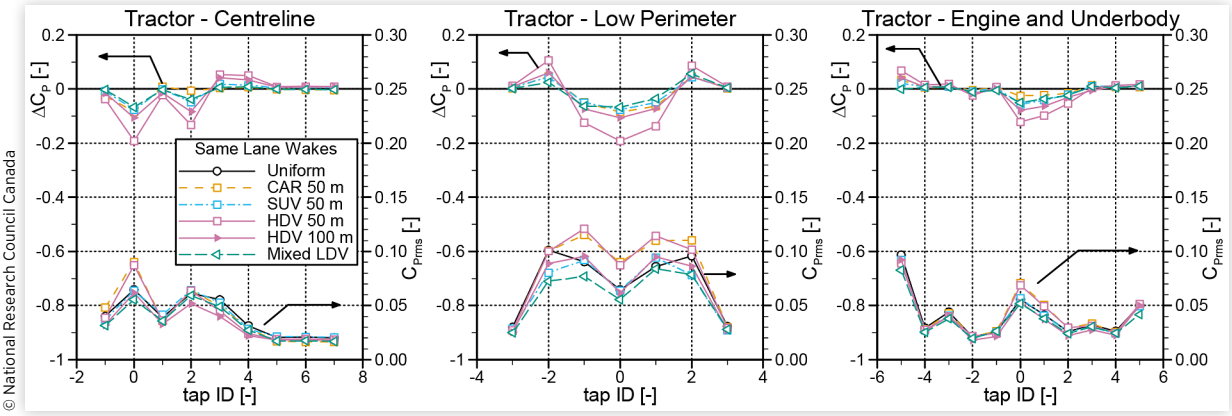

FIGURE 18 Tractor surface-pressure-coefficient measurements for the SCDV-SK configuration in same-lane-vehicle wake flows at 4.5° yaw angle (those results found in Figure 13). ΔC_P is relative to uniform-flow at the same yaw angle. Measurement uncertainty is of the size of the symbols or smaller for the C_P values (approximately ±0.02) and double the symbol size for the C_{Prms} values (approximately ±0.01).

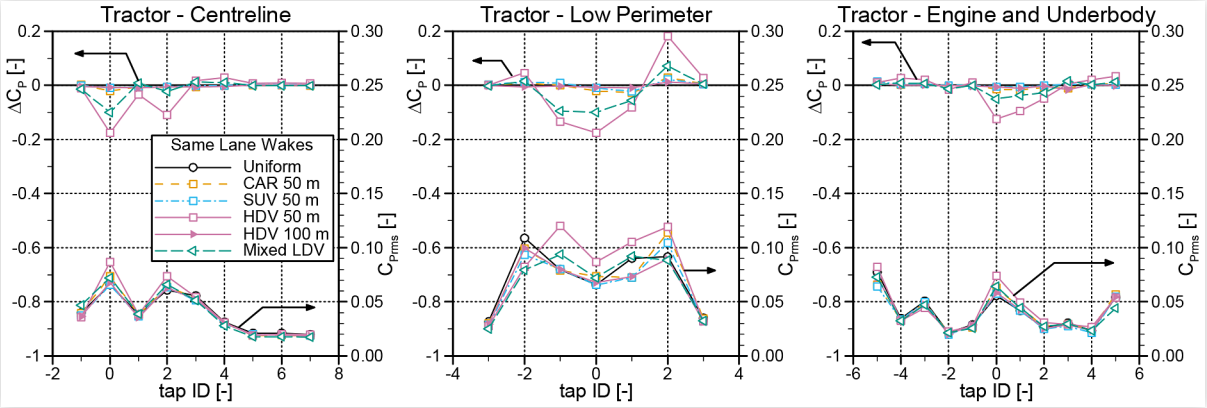

For wakes associated with vehicles in an adjacent lane, only a small influence on tractor surface pressures is observed at 0° yaw angle (Figure 19). Here, the Mixed LDV case has the largest influence, but only because that case simulates a condition with vehicles in the same and adjacent lanes, thus the effects can be primarily attributed to the same-lane vehicle. At this yaw angle, the HDV wake cases (50mand 100 m) induce small but measurable changes in the surface pressures because the wakes are so large that they encroach into the adjacent lane.

The most significant influences to the tractor surface pressures are observed at a yaw angle of 7.5° for adjacent-lane conditions, shown in Figure 20. This is the condition for which the largest drag reduction was noted, for the HDV 50mcase, based on data in Figure 16. All cases show effects on C_P up to at least windshield height (centreline tap ID +2), and all show an asymmetric low-perimeter distribution consistent with an effective reduction in yaw angle. The largest ΔC_P magnitude change of the entire data set, of 0.3, is observed for the HDV 50 m case for low-perimeter tap ID -1, with the highest tractor C_{Prms} value of 0.15 observed for low-perimeter tap ID -2 noted for this case as well. Although downplayed earlier when discussing the trailer surface-pressure-results, small but measurable ΔC_P values are observed on the trailer at this 7.5°-yaw-angle condition for the CAR 25 m, SUV 25 m, HDV 50 m and Mixed LDV cases. These quantifiable changes are observed in the underbody and bogie region for many of the forward-facing taps (tap IDs -5, -4, -3, 0, +1, +2, +4, +5, and +6) with reductions in C_P relative to the uniform-flow results, indicating a possible reduction in the wind speed through the underbody region.

In contrast to the tractor, the trailer surface-pressure results show small or negligible changes in pressure coefficients, both mean and rms, associated with the wake flows. This is evident in Figure 21 for the adjacent-lane 7.5°-yaw-angle conditions for the trailer-with-skirts (SK) configuration. This example shows some of the largest trailer-C_P differences observed in the larger data set. Small differences are observed over the aft half or underbody/bogie region of the trailer, more so for the rms coefficients than the mean values.

The results discussed in this section, and highlighted by the previous paragraph, show that traffic wakes influence the

FIGURE 19 Tractor surface-pressure-coefficient measurements for the SCDV-SK configuration in adjacent-lane-vehicle wake flows at 0° yaw angle. ΔC_P is relative to uniform-flow at the same yaw angle (those results found in Figure 12). Measurement uncertainty is of the size of the symbols or smaller for the C_P values (approximately ±0.02) and double the symbol size for the C_{Prms} values (approximately ±0.01).

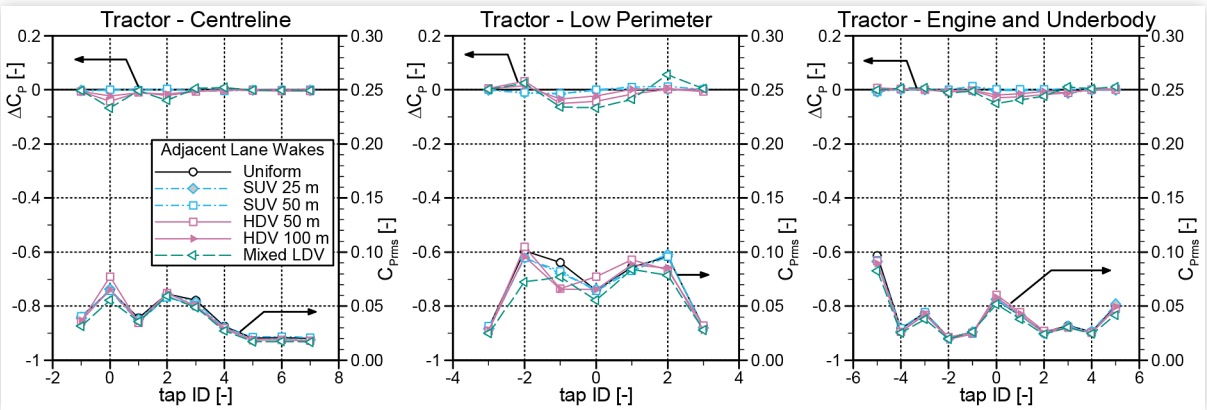

FIGURE 20 Tractor surface-pressure-coefficient measurements for the SCDV-SK configuration in adjacent-lane-vehicle wake flows at 7.5° yaw angle. ΔC_P is relative to uniform-flow at the same yaw angle (those results found in Figure 14). Measurement uncertainty is of the size of the symbols or smaller for the C_P values (approximately ±0.02) and double the symbol size for the C_{Prms} values (approximately ±0.01).

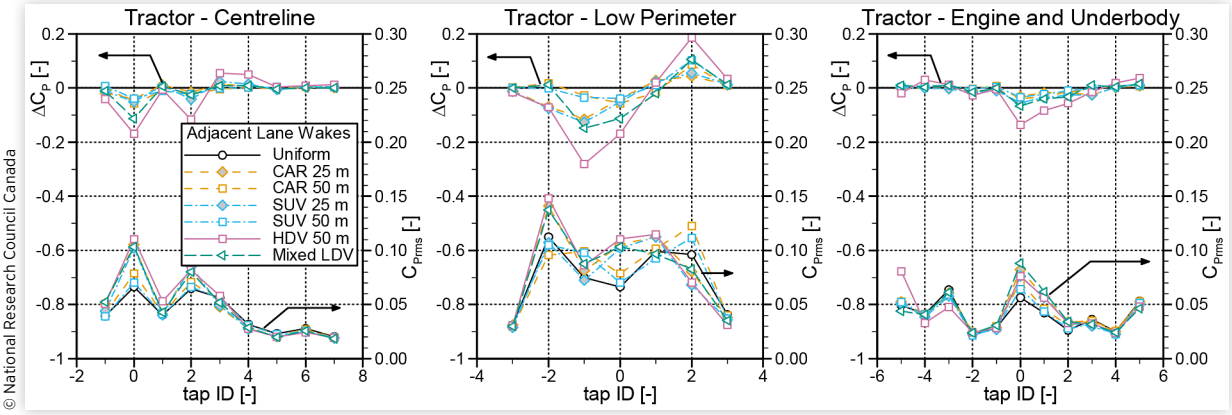

FIGURE 21 Trailer surface-pressure-coefficient measurements for the SCDV-SK configuration in adjacent-lane-vehicle wake flows at 7.5° yaw angle. ΔC_P is relative to uniform-flow at the same yaw angle (those results found in Figure 14). Measurement uncertainty is of the size of the symbols or smaller for the C_P values (approximately ±0.02) and double the symbol size for the C_{Prms} values (approximately ±0.01).

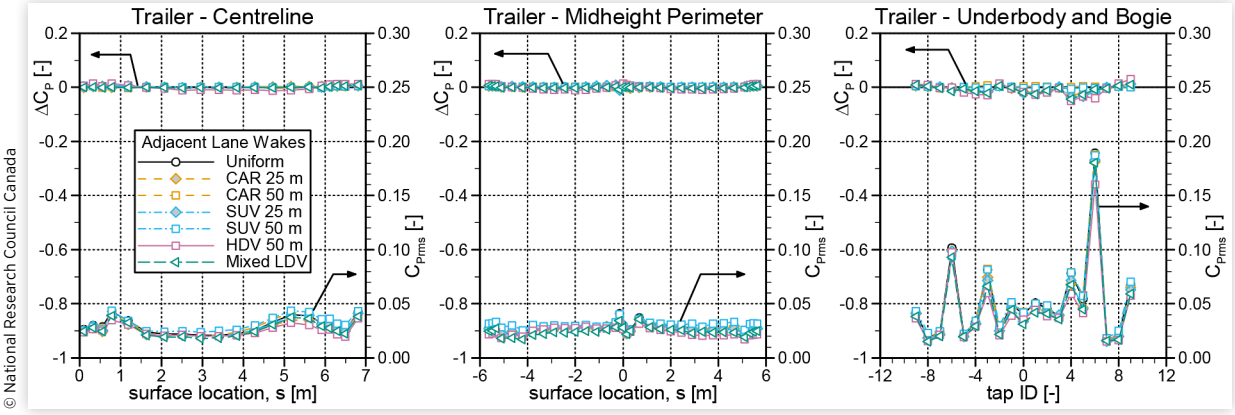

pressures predominantly over forward-facing surfaces of the HDV model which, in turn, influence the wind loads experienced by these vehicles on the road. These results also explain why the drag coefficient, of all the force/moment coefficients, is most influenced by wake effects, given that it is dominated by effective differences in surface pressures between the front and back surfaces of the vehicle. Other force/moment coefficients that show influences from wake effects, namely side force and rolling moment, appear to be influenced more so by effective changes in yaw angle due to flow-directionality changes in the wakes.

Influence of Wake Effects on HDV Configuration Changes

Thus far, a single HDV configuration has been used to demonstrate the influence of traffic wakes on the aerodynamic performance. This approach was selected due to a general similarity observed for all ten HDV configurations tested. However, some differences in wake effects have been identified amongst HDV configurations, and this section documents those differences.

The drag-coefficient data for all ten vehicle configurations in all tested wake flows are provided in Figures 22–25, with each of the four figures representing one of the four primary HDV configurations with its variants. The two columns represent the wake-source lane location: same-lane on the left and adjacent-lane on the right. The same trend emerges in each respective lane plot, with the reduction in C_D from the wake flows showing the same patterns relative to each other, with the CAR wake producing the smallest influence and the HDV wakes providing the largest influence. In addition, a larger difference between a given wake condition and the corresponding uniform-flow results is observed for HDV configurations with higher uniform-flow C_D values, showing proportionally-similar differences as will be discussed later in this section.

FIGURE 22 Drag-coefficient measurements for the sleeper-cab tractor with dry-van trailer variants. HDV configurations top to bottom: SCDV-SR, SCDV-SK, SCDV-BT, SCDV-LD. Left plot: same-lane wakes. Right plot: adjacent-lane wakes. Measurement confidence interval is the size of the symbols.

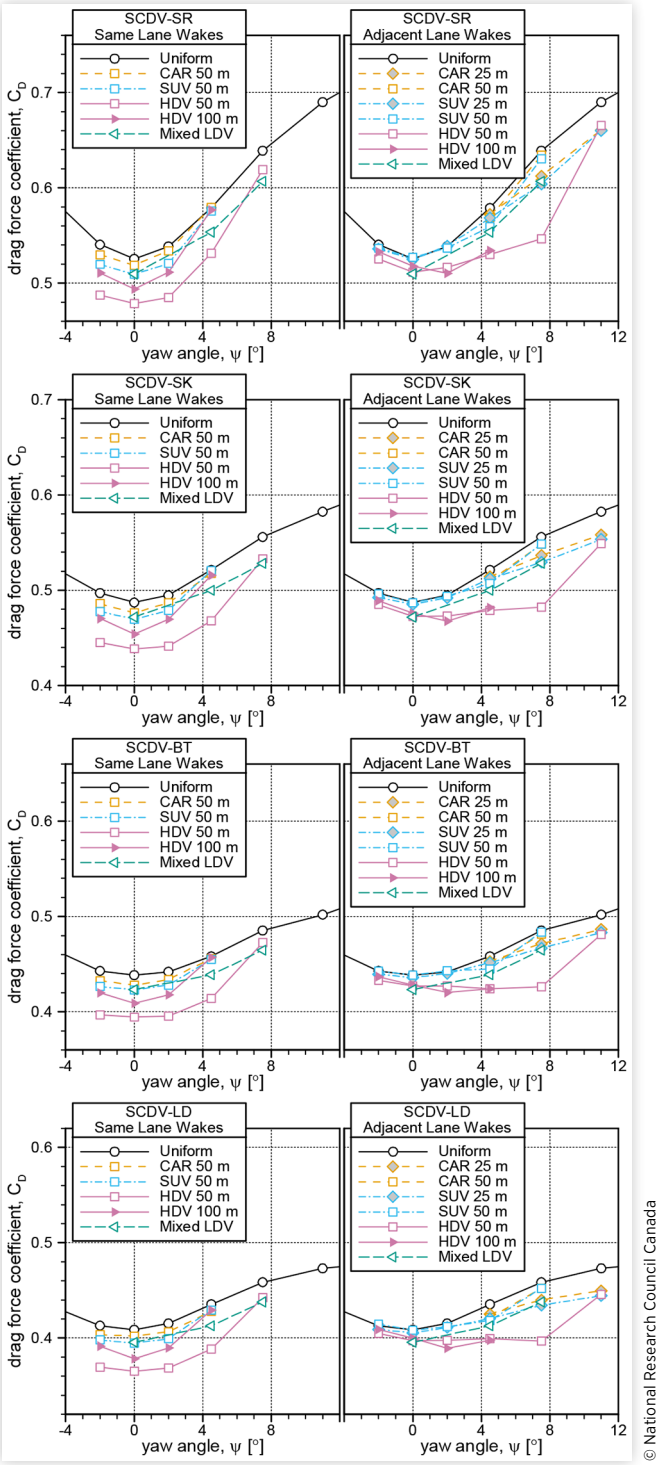

FIGURE 23 Drag-coefficient measurements for the day-cab tractor with dry-van trailer variants. HDV configurations top to bottom: DCDV-SR, DCDV-SK, DCDV-BT. Left plot: same-lane wakes. Right plot: adjacent-lane wakes. Measurement confidence interval is the size of the symbols.

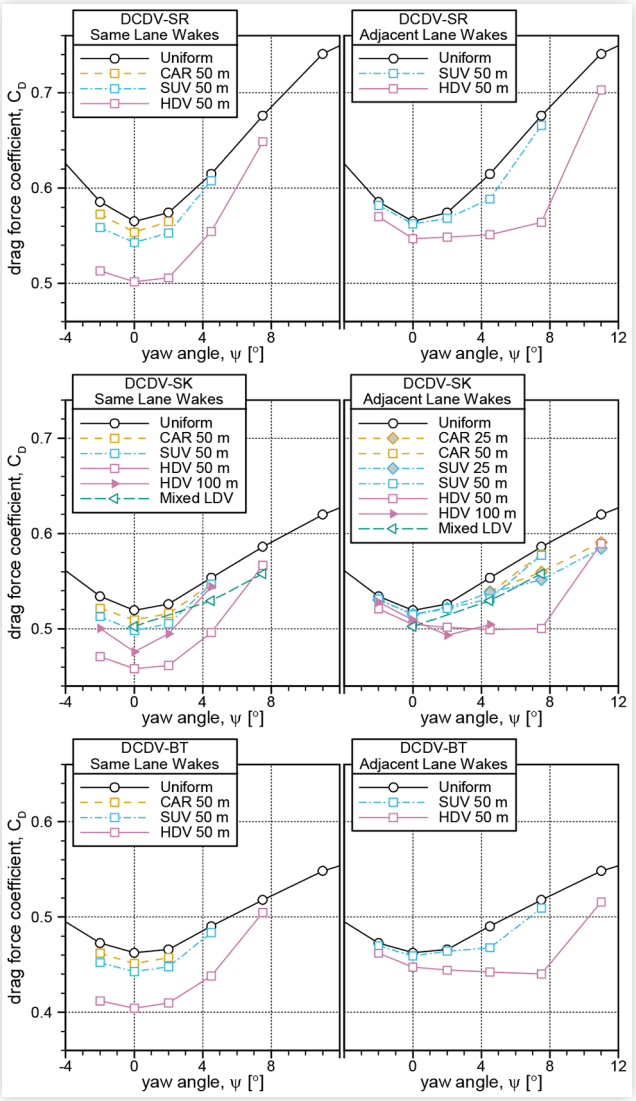

An interesting feature of the results presented here, highlighted by the adjacent-lane HDV 50 m results, is the insensitivity of C_D to yaw angle for many of the tested HDV configurations for yaw angles between 0° and 7.5°. This is more prevalent for the day-cab and zero-emission-cab results of Figures 23 through 24 than for the sleeper-cab results in Figure 22, the latter showing this for only the two lowest drag configurations (BT and LD). Of particular note is the day-cab-with-flat-bed configuration (Figure 25) that shows the minimum adjacent-lane C_D values occurring at a yaw angle of 7.5° for both the empty and box-cargo configurations with the HDV 50 m wake condition. This arises due to the lower general sensitivity to yaw-angle of the uniform-flow results for these HDV configurations resulting, it is suspected, from the lower side area of these configurations compared to the dry-van configurations. For the empty-flatbed configuration (DCFB-EM), the adjacent-lane results show C_D minima at yaw angles of 4.5° or 7.5° for the SUV 25 m, SUV 50 m, HDV 50mand HDV 100mcases. These minima are nearly as low as their equivalent minimum same-lane wake-flow C_D values.

FIGURE 24 Drag-coefficient measurements for the zero-emissions-cab tractor with dry-van trailer variant (ZEDV-SK). Left plot: same-lane wakes. Right plot: adjacent-lane wakes. Measurement confidence interval is the size of the symbols.

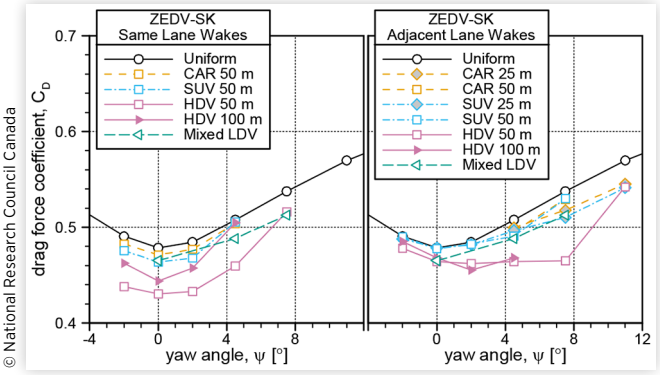

FIGURE 25 Drag-coefficient measurements for the day-cab tractor with flat-bed trailer variants. HDV configurations top to bottom: DCFB-EM, DCFB-BC. Left plot: same-lane wakes. Right plot: adjacent-lane wakes. Measurement confidence interval is the size of the symbols.

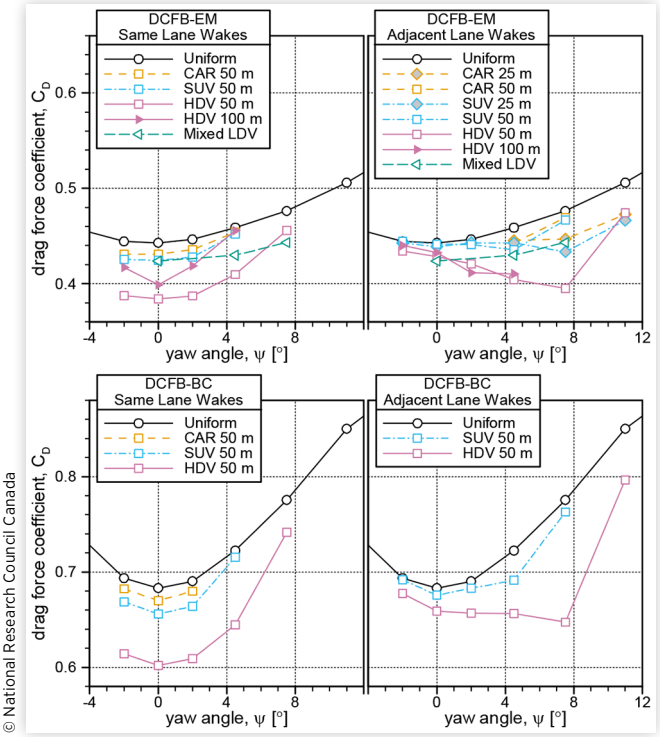

A question to consider from these data is whether changes in C_D for a given change in tractor or trailer configuration are the same in wake effects as they are in uniform flow. Due to the large number of data points for each HDV configuration, this question is addressed here by first providing some sample results for the differences in individual values (ΔC_D) for two HDV-configuration changes.

The effect of removing side-skirts from the dry-van trailer, with and without wake effects, is presented in Figure 26, based on the sleeper-cab configuration. As with C_D results

FIGURE 26 Drag-coefficient differences with and without wake effects when removing side-skirts from the dry-van trailer, paired with the sleeper-cab tractor. Uncertainty in ΔC_D values is 0.004 (top row) and uncertainty in $\Delta C_{\%D}$-ratio values is 0.15 highlighted by gray bars (bottom row).

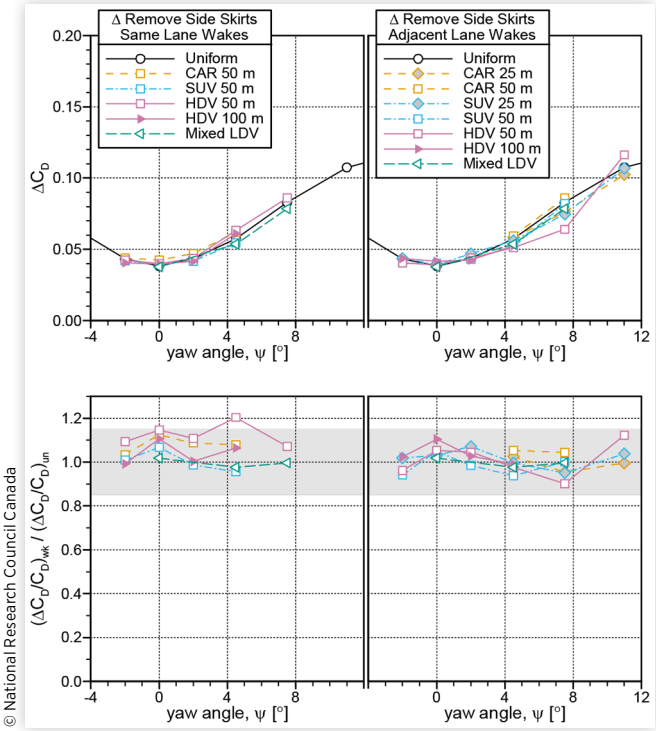

presented in earlier figures, the same-lane-wake results are provided in the left column and the adjacent-lane-wake results in the right column. The top plot show the ΔC_D values associated with removing the side-skirts, which varies from about 0.04 at 0° yaw angle to 0.120 at 15° yaw angle, and with only small differences amongst different flow conditions. Only the adjacent-lane HDV 50 m case exhibits measurable differences at the higher yaw angles. The bottom-row plots show these data in a different format, as the ratio of the proportional ΔC_D changes, relative to the respective flow-referenced baseline configuration, and permits an improved assessment of the effects relative to measurement uncertainties. The compounding of incremental uncertainties in each parameter makes it difficult to assess whether observed differences in the measurement results are reliable. These large uncertainties are represented by the gray bands that identify the range outside of which these values must fall to be considered a quantifiable difference. Here, only a single value (same-lane HDV 50 m at 4.5° yaw angle) falls outside this range. This suggests that, within the experimental uncertainty of the current experiments ($\delta\Delta C_D = \pm 0.004$), the drag-coefficient impact of removing trailer skirts from an HDV in wake effects may be understood from uniform-flow measurements alone, in an appropriately-scaled manner. This finding is representative of the various trailer-change results of the current study.

A second sample case is presented in Figure 27, showing the effects of changing the tractor from the sleeper-cab to the

FIGURE 27 Drag-coefficient differences with and without wake effects when changing from the sleeper-cab tractor to the day-cab tractor, paired with the skirts-outfitted dry-van trailer. Uncertainty in ΔC_D values is 0.004 (top row), and uncertainty in $\Delta C_{\%D}$-ratio values is 0.18 highlighted by gray bars (bottom row).

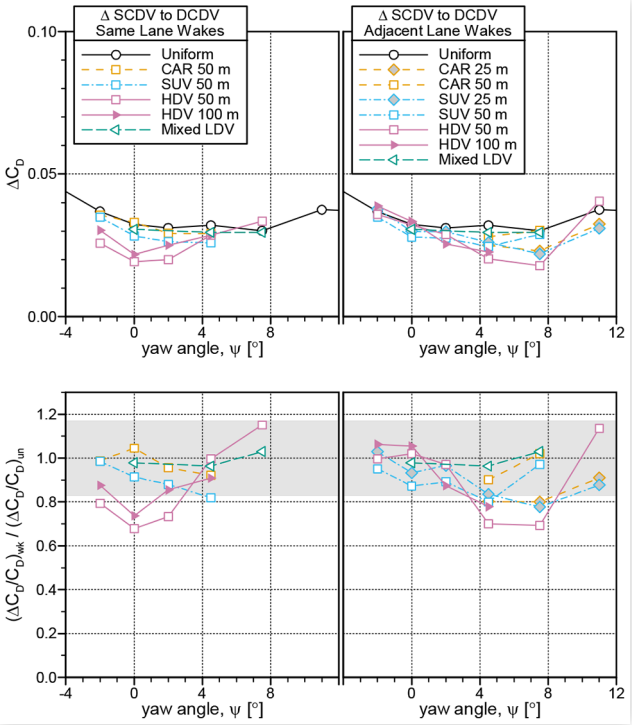

daycab variant. Asymmetry about 0° yaw angle is observed in these

ΔC_D results, arising from different levels of yaw asymmetry associated with these two tractor models. This asymmetry difference is also observed in the uniform-flow results presented earlier in Figure 11. In the ΔC_D results of Figure 27, there are greater differences amongst the different flow conditions than were observed for the trailer-change results of Figure 26. The ΔC_D-ratio parameter in the bottom-row plots highlight this, with CAR, SUV, and HDV wakes showing quantifiable changes at some yaw-angle conditions, despite the compounded uncertainties.

Results from the two sample model changes presented, one for the trailer and one for the tractor, are consistent with the surface-pressure measurements that showed small influence of the wakes on the flow surrounding the trailer model and measurable changes to the flow around the tractor model.

Conclusions

This paper has presented an experimental study of wake effects applied to HDVs in simulated on-road safe-distance traffic conditions. Ten HDV configurations were tested, each in up to 53 wake-flow conditions generated by the RT2S representing different traffic-vehicle types, effective distances, relative lane position, and freestream yaw angles. Wind-load and surface-pressure measurements were presented to examine changes in the aerodynamic performance of the HDV-model configurations relative to uniform-wind conditions. Findings of the study include:

- All of the simulated vehicle-wake types, including the individual compact-sedan (CAR) wake, demonstrated measurable reductions in the drag coefficient of the HDV models for some, or all, of the yaw angles at which data were acquired for each type. Drag-coefficient reductions up to 17% for individual C_D values and up to 9% for wind-averaged values were observed. The drag reductions were observed for effective vehicle distances that are experienced in everyday traffic.
- Multi-LDV wake scenarios can affect the aerodynamic performance of an HDV model over a wider range of yaw angles than the individual-vehicle wakes of which they are comprised.
- In cross winds, the redirection of flow in the wakes can reduce the effective yaw angle at which the following vehicle operates, with associated reductions in drag-force, side-force and rolling-moment coefficients.
- The lift-force, pitching moment, and yawing-moment coefficients of the HDV models are not influenced in a significant manner by the wakes of forward vehicles.
- In cross winds, the wakes from adjacent-lane vehicles can affect the aerodynamic performance of an HDV to a similar or greater extent than the wakes from a same-lane vehicle in no-wind/head-wind/tail-wind conditions.
- Wakes were shown to measurably influence drag-coefficient-difference values at individual yaw angles mainly for tractors changes, with differences from trailer changes generally within the experimental uncertainty.

These results represent the first comprehensive study of traffic-wake effects on HDVs at safe inter-vehicle distances in highway-driving conditions. They highlight significant potential differences in real-world aerodynamic performance relative to the standard wind-averaged uniform-flow metrics used for fuel/energy-use and GHG-emissions predictions. To provide a means of quantifying large-scale traffic effects for such purposes, methods should be developed to account for traffic influences without the necessity for experimental and/or computational evaluation of a large range of specific wake and cross-wind conditions. The development of a *wind-and-traffic*-averaged drag coefficient that can be applied to uniform-flow performance results should be investigated for widespread adoption of the traffic-wake influence in aerodynamic-performance quantification.

In addition to examining the potential for defining a *wind-and-traffic*-averaged drag coefficient, the next steps of this research initiative involve using these data as a basis for predicting wake effects more generally. This includes a similar study planned for LDV vehicle types at 30% scale using the RT²S, which is expected to show greater sensitivity to the simulated wakes than the HDV results presented herein. Furthermore, a combination of wake-flow measurements that were acquired for the various RT²S configurations will

be analyzed for the potential of defining an effective flow condition (a reduced wind speed and reduced yaw angle) that can be used to scale uniform-flow results for estimating traffic-wake influences. Combined with a general-traffic wake-prediction model being developed by this research team, the intention is to develop an analysis methodology to predict and optimize the performance of road vehicles from a traffic-aerodynamics perspective.

Acknowledgements

This work was co-funded by Transport Canada's ecoTECHNOLOGY for Vehicles program and the National Research Council Canada's Clean and Energy Efficient Transportation program. The views and opinions of the authors expressed herein do not necessarily state or reflect those of Transport Canada.

References

1. Wang, Z., Bian, Y., Shladover, S.E., Wu, G. et al., "A Survey on Cooperative Longitudinal Motion Control of Multiple Connected and Automated Vehicles," *IEEE Intelligent Transportation Systems Magazine* (2019).
2. Liu, H., Shladover, S.E., and Kan, X.L.X., "Freeway Vehicle Fuel Efficiency Improvement via Cooperative Adaptive Cruise Control," *Journal of Intelligent Transportation Systems* (2020), doi:10.1080/15472450.2020.1720673.
3. Paddeu, D. and Denby, J., "Decarbonising Road Freight: Is Truck Automation and Platooning an Opportunity?" *Clean Technologies and Environmental Policy* (2020), doi:10.1007/s10098-020-02020-9.
4. Zhang, L., Chen, F., Ma, X., and Pan, X., "Fuel Economy in Truck Platooning: A Literature Overview and Directions for Future Research," *Journal of Advanced Transportation* (2020), doi:10.1155/2020/2604012.
5. Le Good, G., Resnick, M., Boardman, P., and Clough, B., "Effects on the Aerodynamic Characteristics of Vehicles in Longitudinal Proximity Due to Changes in Style," SAE Technical Paper 2018-37-0018 (2018), https://doi.org/10.4271/2018-37-0018.
6. McAuliffe, B.R. and Ahmadi-Baloutaki, M., "A Wind-Tunnel Investigation of the Influence of Separation Distance, Lateral Stagger, and Trailer Configuration on the Drag-Reduction Potential of a Two-Truck Platoon," *SAE Int. J. Commer. Veh.* 11, no. 2 (2018): 125-150, https://doi.org/10.4271/02-11-02-0011.
7. Tadakuma, K., Doi, T., Shida, M., and Maeda, K., "Prediction Formula of Aerodynamic Drag Reduction in Multiple-Vehicle Platooning Based on Wake Analysis and On-Road Experiments," *SAE Int. J. Passeng. Cars - Mech. Syst.* 9, no. 2 (2016): 645-656, https://doi.org/10.4271/2016-01-1596.
8. Salari, K. and Ortega, J., "Experimental Investigation of the Aerodynamic Benefits of Truck Platooning," SAE Technical Paper 2018-01-0732 (2018), https://doi.org/10.4271/2018-01-0732.
9. McAuliffe, B.R., Smith, P., Raeesi, A., Hoffman, M. et al., "Track-Based Aerodynamic Testing of a Two-Truck Platoon," *SAE Int. J. Advances & Curr. Prac. in Mobility* 3, no. 3 (2021): 1450-1472, https://doi.org/10.4271/2021-010941.
10. Eskridge, R.E. and Thompson, R.S., "Experimental and Theoretical Study of the Wake of a Block-Shaped Vehicle in a Shear-Free Boundary Flow," *Atmospheric Environment* 16, no. 12 (1982): 2821-2836.
11. Baker, C.J., "Flow and Dispersion in Ground Vehicle Wakes," *Journal of Fluids and Structures* 15 (2001): 1031-1060.
12. McAuliffe, B.R., Sowmianarayanan, B., and Barber, H., "Near-to-Far Wake Characteristics of Road Vehicles Part 2: Influence of Cross Winds and Free-Stream Turbulence," *SAE Int. J. Advances & Curr. Prac. in Mobility* 3, no. 4 (2021): 2046-2068, https://doi.org/10.4271/2021-01-0949.
13. Watkins, S. and Vino, G., "The Effect of Vehicle Spacing on the Aerodynamics of a Representative Car Shape," *Journal of Wind Engineering and Industrial Aerodynamics* 96 (2008): 1232-1239.
14. McAuliffe, B.R. and Barber, H., "Simulating Traffic-wake Effects in a Wind Tunnel," SAE Paper Submission 23SS-0195, 2023.
15. Jessing, C., Wilhelmi, H., Wittmeier, F., Wagner, A. et al., "Investigation of Transient Aerodynamic Effects on Public Roads in Comparison to Individual Driving Situations on a Test Site," *SAE Int. J. Adv. & Curr. Prac. in Mobility* 2, no. 5 (2020): 2585-2595, https://doi.org/10.4271/2020-01-0670.
16. McAuliffe, B.R. and D'Auteuil, A., "A System for Simulating Road-Representative Atmospheric Turbulence for Ground Vehicles in a Large Wind Tunnel," *SAE Int. J. Passeng. Cars - Mech. Syst.* 9, no. 2 (2016): 817-830, https://doi.org/10.4271/2016-01-1624.
17. McAuliffe, B.R., Sowmianarayanan, B., and Barber, H., "Near-to-Far Wake Characteristics of Road Vehicles Part 1: Influence of Ground Motion and Vehicle Shape," *SAE Int. J. Advances & Curr. Prac. in Mobility* 3, no. 4 (2021): 2009-2024, https://doi.org/10.4271/2021-01-0957.
18. McAuliffe, B.R., Sowmianarayanan, B., and Barber, H., "Near-to-Far Wake Characteristics of Road Vehicles Part 3: Influence of Multi-Vehicle Interactions," *SAE Int. J. Advances & Curr. Prac. in Mobility* 3, no. 4 (2021): 2025-2045, https://doi.org/10.4271/2021-01-0959.
19. SAE J1252, "SAE Wind Tunnel Test Procedure for Trucks and Busses." Surface Vehicle Recommended Practice J1252," 2012.
20. US Environmental Protection Agency and US Department of Transportation, "Greenhouse Gas Emissions Standards and Fuel Efficiency Standards for Medium- and Heavy-Duty Engines and Vehicles - Phase 2," US Federal Register 81(206):73478–74274, 2016.
21. McAuliffe, B.R., Ghorbanishohrat, F., and Barber, H., "Preliminary Investigation Towards Next Generation Truck Design for Aerodynamic Efficiency," NRC Report LTR-AL-2022-0069, 2022.
22. Waltzer, S., Hawkins, J., Mitcham, A., Lock, A. et al., "Wind Tunnel Evaluation of Potential Aerodynamic Drag Reductions from Trailer Aerodynamic Component Combinations," SAE Technical Paper 2015-01-2884 (2015), https://doi.org/10.4271/2015-01-2884.

23. McAuliffe, B.R., "Improving the Aerodynamic Efficiency of Heavy Duty Vehicles: Wind Tunnel Test Results of Trailer-Based Drag-Reduction Technologies," NRC Report LTRAL-2017-0272, National Research Council Canada, 2015.
24. McAuliffe, B.R., Raeesi, A., Lammert, M.P., Smith, P. et al., "Impact of Mixed Traffic on the Energy Savings of a Truck Platoon," *SAE Int. J. Advances & Curr. Prac. in Mobility* 2, no. 3 (2020): 1472-1496, https://doi.org/10.4271/2020-01-0679.
25. McAuliffe, B.R., Lammert, M., Lu, X., Shladover, S. et al., "Influences on Energy Savings of Heavy Trucks Using Cooperative Adaptive Cruise Control," SAE Technical Paper 2018-01-1181 (2018), https://doi.org/10.4271/2018-01-1181.
26. Lammert, M.P., McAuliffe, B.R., Raeesi, A., Smith, P. et al., "Impact of Lateral Alignment on the Energy Savings of a Truck Platoon," SAE Technical Paper 2020-01-0594 (2020), https://doi.org/10.4271/2020-01-0594.

e-ISSN 2641-9645